

THE HOST GALAXIES OF FAST-EJECTA CORE-COLLAPSE SUPERNOVAE

PATRICK L. KELLY¹, ALEXEI V. FILIPPENKO¹, MARYAM MODJAZ², AND DANIEL KOCEVSKI³*Submitted to The Astrophysical Journal*

ABSTRACT

Spectra of broad-lined Type Ic supernovae (SN Ic-BL), the only kind of SN observed at the locations of long-duration gamma-ray bursts (LGRBs), exhibit wide features indicative of high ejecta velocities ($\sim 0.1c$). We study the host galaxies of a sample of 245 low-redshift ($z < 0.2$) core-collapse SN, including 17 SN Ic-BL, discovered by galaxy-untargeted searches, and 15 optically luminous and dust-obscured $z < 1.2$ LGRBs. We show that, in comparison with SDSS galaxies having similar stellar masses, the hosts of low-redshift SN Ic-BL and $z < 1.2$ LGRBs have high stellar-mass and star-formation-rate densities. Core-collapse SN having typical ejecta velocities, in contrast, show no preference for such galaxies. Moreover, we find that the hosts of SN Ic-BL, unlike those of SN Ib/Ic and SN II, exhibit high gas velocity dispersions for their stellar masses. The patterns likely reflect variations among star-forming environments, and suggest that LGRBs can be used as probes of conditions in high-redshift galaxies. They may be caused by efficient formation of massive binary progenitors systems in densely star-forming regions, or, less probably, a higher fraction of stars created with the initial masses required for a SN Ic-BL or LGRB. Finally, we show that the preference of SN Ic-BL and LGRBs for galaxies with high stellar-mass and star-formation-rate densities cannot be attributed to a preference for low metal abundances but must reflect the influence of a separate environmental factor.

Subject headings: gamma rays: bursts — supernovae: general — galaxies: star formation — galaxies: abundances

1. INTRODUCTION

In the cases of at least ten nearby (redshift $z \lesssim 0.5$) LGRBs, observations have revealed a SN Ic-BL spectrum superimposed on the power-law continuum of the fading optical afterglow (Galama et al. 1998; Matheson et al. 2003; Stanek et al. 2003; Hjorth et al. 2003; see Woosley & Bloom 2006 and Modjaz 2011 for reviews). The spectra are characterized by wide features consistent with high ejecta velocities ($\sim 20,000\text{--}30,000\text{ km s}^{-1}$), and an absence of hydrogen and helium. The other principal classes of core-collapse SN, in contrast, exhibit spectroscopic features consistent with more slowly moving ejecta. The most common core-collapse SN are Type II ($\sim 60\%$; Li et al. 2011; Smartt et al. 2009), which exhibit hydrogen (H) in their spectra; they are the final eruptions of stars that have retained their outer H shell. When the progenitor sheds, transfers to a companion, or internally mixes its outer H envelope during pre-SN evolution, the explosion will produce an H-deficient SN Ib, or an H- and He-deficient SN Ic (e.g., Filippenko 1997, and references therein).

While the absence of H and He in the spectra of SN Ic-BL indicates that their progenitors have lost their envelopes prior to core collapse, simulations additionally suggest that the progenitors of SN Ic-BL with associated LGRBs may also have rapid speeds of rotation. In models, only quickly rotating stars without an H envelope produce the outflowing jets that yield γ -ray emission (Hirschi et al. 2005; Yoon & Langer 2005; Langer & Norman 2006) after core collapse to a black hole (Woosley et al. 1993; MacFadyen & Woosley 1999).

Close massive binary systems that experience mass trans-

fer, common-envelope evolution, or a merger (Podsiadlowski et al. 2010; Langer 2012) are possible progenitors of LGRBs, because they can likely produce the required rapidly rotating massive stars without H or He envelopes. Recent observations of Galactic O-type stars show that, in fact, $\gtrsim 70\%$ of massive stars experience mass transfer with a companion and $\sim 30\%$ undergo a merger (Sana et al. 2012). Alternative progenitor candidates include quickly rotating, metal-poor stars that internally mix their outer envelopes (Yoon & Langer 2005; Woosley & Heger 2006). Single stars with high abundances, however, are considered improbable progenitors, because their comparatively strong winds (Vink et al. 2001) are expected to reduce their angular momentum.

Spectroscopy of $z \lesssim 0.3$ host galaxies shows, in fact, that nearby SN Ic-BL with an associated GRB prefer more metal-poor environments than nearby Type Ic-BL SN having no obvious γ -ray emission (Modjaz et al. 2008; Kocevski et al. 2009; Graham & Fruchter 2013). The latter, in turn, prefer more metal-poor (Kelly & Kirshner 2012; Sanders et al. 2012) and blue (Kelly & Kirshner 2012) environments than do SN Ic without broad features.

In several cases, however, the positions of low- and moderate-redshift LGRBs are spatially coincident or closely associated with massive, metal-rich galaxies (e.g., Levesque et al. 2010; Perley et al. 2013; Elliott et al. 2013). Absorption spectroscopy also finds evidence for high-redshift $z \gtrsim 2$ systems along the line of sight to LGRBs with metallicities exceeding the $z \gtrsim 2$ cosmic average (Prochaska et al. 2007). Savaglio et al. (2012) has inferred a supersolar abundance from $z = 3.57$ absorption features consistent with a pair galaxies in the GRB 090323 afterglow spectrum. GRB 130702A (Singer et al. 2013) occurred, however, in a metal-poor faint satellite of a $z = 0.145$ massive galaxy (Kelly et al. 2013), raising the possibility of superpositions or associations for some LGRBs that would be difficult to resolve at high redshift.

Here we measure the host-galaxy properties of nearby

¹ Department of Astronomy, University of California, Berkeley, CA 94720-3411, USA

² CCPP, New York University, 4 Washington Place, New York, NY 10003, USA

³ NASA/Goddard Space Flight Center, Code 662, Greenbelt, MD 20771, USA

($z < 0.2$) core-collapse SN explosions using the imaging and photometry of the Sloan Digital Sky Survey (SDSS). For $z < 1.2$ LGRB hosts, we estimate these host properties from published photometry and archival *HST* images. We show that SN Ic-BL and LGRBs exhibit a strong preference for galaxies that have high stellar-mass density and star-formation-rate density for their stellar mass. We also use SDSS spectra to show that the gas kinematics of SN Ic-BL hosts are exceptional. In §2, we describe the core-collapse SN and LGRB samples as well as the SDSS and *HST* galaxy data that we use in this analysis. Section 3 presents our techniques to analyze the galaxy imaging and spectroscopy, and the statistical methods we employ. In §4, we describe the results of our analysis, while §5 discusses the interpretation of the observed patterns. Our conclusions are presented in §6.

2. DATA

We study the host galaxies of both nearby ($z < 0.2$) core-collapse SN discovered by “galaxy-untargeted” transient searches (e.g., the Palomar Transient Factory; PTF; Rau et al. 2009; Law et al. 2009) which do not target specific potential hosts, and $z < 1.2$ LGRBs detected by γ -ray satellites. We use the SDSS spectroscopic sample to build a control sample of low-redshift star-forming galaxies, and SDSS photometry and spectroscopy to measure properties of both the sample of low-redshift star-forming galaxies and the host galaxies of the nearby SN. For the host galaxies of $z < 1.2$ LGRBs, we estimate host properties using published photometry and *HST* imaging.

2.1. SDSS DR10 Photometry and Spectroscopy

The SDSS galaxy photometry and fiber spectra are from Data Release 10 (DR10; Ahn et al. 2013), and they were collected with the 2.5 m telescope at Apache Point, New Mexico. The imaging survey, which spans 14,555 square degrees, consists of 53.9 s integrations through the SDSS *ugriz* filters, and the typical limiting *r*-band AB magnitude is 22.2. The typical sensitivity of available SDSS imaging makes possible detection of $z = 0.1$ galaxies with absolute Vega magnitudes M_B or M_V brighter than about -15.2 . Each Sloan 2048 \times 1498 pixel CCD array records a $13.5' \times 9.9'$ field of view.

The SDSS spectroscopic survey acquired approximately 45 min of total integration in clear conditions, split into a series of three successive exposures. The spectrograph comprises $3''$ ($2''$ for BOSS) diameter fiber-optic cables placed at the positions of targets on the focal plane. Adjacent fibers can be no closer than $55''$ in a single fiber mask because of engineering constraints (Strauss et al. 2002), and the SDSS spectrographs record light with wavelengths 3800–9200 Å.

The targets selected for SDSS fiber spectroscopy consist of three primary “Legacy” categories of objects, and were also taken from several dozen ancillary programs, some of which were limited to specific parts of the survey (e.g., Stripe 82). Objects detected with 5σ significance in the imaging survey, with an extended light distribution and having *r*-band magnitude brighter than 17.77, as well as QSO candidates and luminous red galaxies (LRGs), formed the Legacy samples (Baldry et al. 2005). More limited special-program science targets included, for example, a *u*-band galaxy sample selected to investigate the properties of blue, faint galaxies.

Table 1 shows the construction of our sample of SDSS galaxy spectra.

2.2. Transient and Host-Galaxy Samples

2.2.1. Nearby SN Sample

The core-collapse SN sample is constructed from $z < 0.2$ discoveries by SN surveys that do not target specific galaxies. The “galaxy-untargeted” SN search technique is akin to that of wide-field γ -ray satellite (e.g., *Swift*) searches for LGRBs. The SN in our sample consist of discoveries by galaxy-untargeted searches reported to the International Astronomical Union (IAU), as well as those published (Arcavi et al. 2010) or reported via Astronomical Telegrams by the PTF, from 1990 January 1 through 2012 May 10. The SN searches that we considered to be galaxy-untargeted are identical those listed by Kelly & Kirshner (2012). Our sample consists of only those nearby SN whose host galaxies have SDSS *ugriz* imaging and, when appropriate, a fiber spectrum.

The probability of detecting a SN in an image depends on the limiting magnitude of the transient search, as well as on the SN distance, luminosity, light-curve shape, and dust attenuation along the line of sight. Comparative analysis of the redshifts of core-collapse SN discovered by galaxy-untargeted searches found no significant evidence that variation among the principal species strongly affects their discovery rate (Kelly & Kirshner 2012).

Kelly et al. (2008) showed that SN Ic are more closely associated with the highest surface brightness regions of their host galaxies than SN Ib, but here we combine these two SN types to assemble a larger sample of stripped-envelope SN that do not show high ejecta velocities. We also show, for comparison, the host of PTF12gzk, a peculiar SN Ic that did not exhibit broad spectroscopic features (Ben-Ami et al. 2012) but in which radio observations found evidence for $\sim 0.3c$ ejecta speeds (Horesh et al. 2013). Lists of the nearby SN and the LGRBs are presented in Tables 2 and 3 (full tables are available in the electronic version).

2.2.2. LGRB Sample

Our LGRB sample includes both objects with a detected optical afterglow, and “dark” bursts without a luminous optical afterglow (Taylor et al. 1998) whose position was determined using their X-ray flux (Cenko et al. 2009; Perley et al. 2009). Analysis of the host galaxies of dark GRBs shows that they are both more massive (Perley et al. 2013) and dust-obscured (Djorgovski et al. 2001; Kloise et al. 2003; Perley et al. 2013) than the hosts of GRBs with detected optical afterglows. The fraction of dark bursts in our sample (2/15) is approximately representative of the fraction of dust-obscured GRBs below the $z = 1.2$ redshift upper limit of our LGRB sample reported by Perley et al. (2013).

We assemble $z < 1.2$ LGRB host galaxies having archival *HST* images from the unobscured LGRBs assembled by Savaglio et al. (2009) and dust-obscured LGRBs assembled by Perley et al. (2013), after rejecting several datasets that showed evidence of residual LGRB light. In many cases, *HST* images were acquired at least a year after the explosion; these are the data we use when available to measure galaxy sizes. When only images taken closer to the time of the GRB are available, we inspect the host galaxy to determine whether evidence for a point source at the explosion site exists. LGRBs exhibit a strong association with the brightest pixels of their hosts (Fruchter et al. 2006), so a potential concern is that we could reject data where the LGRB coincided with a bright star-forming region. In practice, possible confusion was minimal for the data taken within ~ 4 months after the GRB trigger. While we do not expect any significant contamination,

TABLE 1
CONSTRUCTION OF SDSS GALAXY SPECTRA
SAMPLE

Criterion	SDSS Fibers
(1) Full Catalog	948,205
(2) Reliable Line Measurements	910,532
(3) Star Forming (Low or High S/N)	377,763
(4) H α S/N > 20	302,865
(5) Fiber Offset < 0.2 R_P	289,474

NOTE. — SDSS spectroscopic fiber sample construction. SDSS galaxies remaining of each spectroscopic type after applying each inclusion criterion. (1) Spectra in full SDSS catalog; (2) deemed reliable line measurement with no redshift fit warning; (3) spectrum classified as star forming, with low or high S/N, according to its position on the Baldwin, Phillips, & Terlevich (BPT; Baldwin et al. 1981) diagram of the [O III] λ 5007/H β and [N II] λ 6584/H α line ratios and line-flux S/N, respectively; (4) galaxies whose H α line-flux measurements have S/N > 5; and (5) center of the SDSS fiber is within 20% of the Petrosian radius R_P .

here we are interested in the integrated properties of the host galaxy and not the specific region where the LGRB occurred.

Even when an optical afterglow can be detected, identifying a coincident SN in the fading afterglow light curve, or by identifying a SN spectrum superimposed on the power-law afterglow continuum, requires high signal-to-noise ratio (S/N) data. Sufficient follow-up observations have only been possible for LGRBs with $z \lesssim 0.6$. Our GRB sample includes events with and without a detected optical afterglow or coincident SN. Since a representative fraction of the LGRBs in our sample have no optical counterpart, our findings should be robust to the effects of dust obscuration on LGRB detection.

3. METHODS

3.1. Measurements of Galaxy Properties

For both the $z < 0.2$ core-collapse SN and $z < 1.2$ LGRB samples, as well as the SDSS star-forming population, we estimate host-galaxy stellar masses M and photometric star-formation rates (SFRs) by fitting PEGASE2 (Floc & Rocca-Volmerange 1999) stellar population synthesis models to broadband photometry; see Kelly et al. (2010) for detailed information on the star-formation histories and initial-mass functions (IMFs) used. For nearby core-collapse SN host galaxies and the SDSS star-forming population, we fit Sloan *ugriz* magnitudes. The multi-band photometry of the host galaxies of LGRBs was assembled from the GHostS database⁴.

We describe a second, complementary set of SFR estimates in the following section that is available only for the SDSS star-forming spectroscopic sample and which uses both the fiber spectrum and broadband *ugriz* photometry. When comparing among samples, however, we only compare SFR values estimated using the same method.

3.1.1. Analyses of SDSS Galaxy Spectra

Several teams have performed and made available detailed measurements of SDSS galaxy properties from the Sloan photometry and spectroscopy. For the $z < 0.2$ samples of core-collapse SN host galaxies and the SDSS star-forming population, we use SFRs estimated from fitting both spectra and

photometry, and gas velocity dispersions σ_{gas} measured from the H α emission-line profile.

We use the star-forming classifications for SDSS galaxies and hybrid spectroscopic and photometric SFR estimates made available by a collaboration that was both at the Max Planck Institute for Astronomy (MPA) and Johns Hopkins University (JHU) (S. Charlot, G. Kauffmann, S. White, T. Heckman, C. Tremonti, and J. Brinchmann; MPA-JHU). SDSS fiber apertures generally do not cover the entire light distribution of each target galaxy. The MPA-JHU team therefore estimates the total SFR of each galaxy as the sum of the SFR within the fiber aperture determined from fitting the spectrum, and from a fit to the *ugriz* light outside the fiber opening.

We adopt the gas velocity dispersions estimated from SDSS emission-line profiles by the Portsmouth group (Thomas et al. 2013), which apply the public Penalized PiXel Fitting (Capellari & Emsellem 2004) (pPXF) and the Gas and Absorption Line Fitting (Sarzi et al. 2006) (GANDALF v1.5) codes. The velocity dispersion of the gas is estimated from the widths of emission lines (e.g., H α , [O III]), and here we take the dispersion for H α .

3.1.2. Host-Galaxy Sizes

The SDSS Photo pipeline performs separate fits of a de Vaucouleurs $r^{1/4}$ law and an exponential profile to the light distribution of each extended object. The pipeline next finds the linear combination of the two models (holding all parameters except flux fixed) that minimizes the χ^2 statistic. To obtain an estimate of the half-light radius r_{50} , we compute the weighted average of the two components' r_{50} parameters and weight each by its fractional contribution to the total model flux.

We use the GALFIT (Peng et al. 2002) program to perform the same surface-brightness fitting analysis on archival *HST* images of LGRB host galaxies. We apply Source Extractor (SExtractor; Bertin & Arnouts 1996) to drizzled and cosmic-ray-rejected images to estimate object positions, ellipticities, and magnitudes, and these are used as input GALFIT parameters. Extended sources except the LGRB hosts are modeled with Sersic profiles, and the instrument point-spread function (PSF) is used to model stars. The host-galaxy r_{50} estimates show good agreement with existing estimates of r_{50} from profile fitting (Conselice et al. 2005), and with published r_{80} SExtractor measurements (Svensson et al. 2010).

The host galaxy of GRB 020903 is part of a complex association of interacting clumps, so the galaxy is not well approximated by a simple surface-brightness model. An additional complication is that much of the host-galaxy photometry was taken from the ground, where the galaxy components cannot be resolved. We therefore have excluded this host galaxy from the analysis.

The angular diameter of ESO184-G82, the host galaxy of the nearby GRB 980425 ($z = 0.0087$), approximately spans the available *HST* images. The physical resolution of the *HST* data is also substantially higher than that of the images of the SDSS SN host galaxies, or other LGRB hosts. Measurement of the host effective radius from model fitting requires significant imaging area without galaxy light to be able to fit robustly for the background level. We therefore do not include GRB 980425, which does not have SDSS exposures, in the LGRB sample.

The host galaxy of GRB 051022 is also a system with two peaks that may possibly correspond to two strongly interacting galaxies, or else may instead be a galaxy with irregular

⁴ <http://www.grbhosts.org>

morphology. We expect that the SDSS Photo pipeline would be most likely to model the host as a single system, so we construct a GALFIT model that consists of a single galaxy.

3.1.3. Stellar-Mass and Star-Formation Densities Estimates

We calculate the projected stellar-mass density Σ_M and the projected star-formation density Σ_{SFR} from the galaxy stellar mass M and star-formation rate SFR, respectively, and the parameters of the model r -band isophotal ellipse that encloses half of the galaxy light. We compute, for example, $\Sigma_M = \log_{10}(M / 2 / \pi AB)$, where M is the stellar mass (in M_\odot), while A and B are the semimajor and semiminor axes (in kpc) of the isophotal ellipse that contains half of the galaxy r -band flux, determined from fitting its surface-brightness distribution.

3.2. Comparison of Host-Galaxy Properties

3.2.1. Median Relationship for Photometric Host Properties

Photometric magnitudes measured through an appropriate aperture designed to enclose a specific percentage of the host light (e.g., a Petrosian aperture; 1976) can be expected to sample an approximately consistent fraction of galaxy light with increasing distance to sources. Physical properties estimated from broadband fluxes (e.g., stellar mass M) should therefore not exhibit strong aperture biases with increasing redshift in our sample, although the effects of surface-brightness dimming may become important at high redshifts.

To study the properties of galaxies derived from photometric measurements, we therefore find the best-fitting M - Σ_M , M - Σ_{SFR} , M - r_{50} , and SFR- r_{50} relations for the complete $0.03 < z < 0.1$ SDSS star-forming catalog. We fit a second-degree polynomial to the median ordinate value (e.g., Σ_{SFR}) across at least five bins in galaxy stellar mass. We include an additional point at $(\log M, r_{50}) = (0, 0)$ and $(\log \text{SFR}, r_{50}) = (-10, 0)$, respectively, when fitting for the SDSS M -SFR relation so that r_{50} approaches zero for galaxies with negligible stellar mass M or SFR. We use the Main SDSS spectroscopic sample Legacy ‘‘GALAXY’’ targets (i.e., where the 64 bit of the primTarget bitmask was set) to measure median relations of the properties of the low-redshift galaxy population.

3.2.2. Spectroscopic Host Properties

The fixed angular size of SDSS 3'' fibers (or 2'' for the Baryon Acoustic Oscillation Survey; BOSS), in contrast to (for example) a Petrosian aperture, samples a percentage of the light of each extended target that depends on the redshift and intrinsic size of the galaxy. To reach conclusions about spectroscopic measurements that are not sensitive to aperture effects, we apply a separate predictive algorithm that we have developed that yields robust comparisons.

To predict the expected value of an observable (e.g., σ_{gas}) given other host-galaxy properties (e.g., mass M), we perform, for each $z < 0.2$ SN host galaxy, a locally weighted multiple linear least-squares fit to the SDSS catalog. We model the observable of interest O_j as

$$O_j = \sum_{i=0}^n A_i x_{ij}, \quad (1)$$

where j indexes the SDSS galaxies, and each x_{ij} is a galaxy property, a combination (e.g., multiplicative product) of galaxy properties, or unity. For example, we model the gas

velocity dispersion σ_{gas} as

$$\sigma_{\text{gas},j} = A_0 + A_1 \log_{10} M_j + A_2 (\log_{10} M_j)^2 + A_3 \epsilon_j, \quad (2)$$

where M is stellar mass and ϵ is galaxy ellipticity. Each row j of the design matrix A_i^j and O^j is multiplied by the weight $W_j = e^{-u_j}$, where u_j is

$$u_j = \frac{(z_j - z^{\text{SN}})^2}{(0.01)^2} + \log_{10} \left(\frac{M_j}{M^{\text{SN}}} \right)^2 + \frac{(F_{\text{aper},j} - F_{\text{aper}}^{\text{SN}})^2}{(0.1)^2} \quad (3)$$

and z is galaxy redshift. To be able to predict a specific property O_{pred} of each host galaxy (e.g., σ_{gas}) independent of its observed value, O_{obs} , we exclude the host galaxy itself when fitting the predictive model to the properties of SDSS galaxies. This approach assigns greater weight to galaxies with similar observables, and mitigates any possible selection effect with galaxy redshift or fiber fraction.

The best-fit parameters A_i for each fit are used to compute a prediction for the value of the galaxy property, O_{pred} , which can then be compared to the observed value, O_{obs} , as a residual,

$$\Delta O \equiv O_{\text{obs}} - O_{\text{pred}}. \quad (4)$$

Here the fitting analysis requires only modest numbers of nearby datapoints from the SDSS spectroscopic catalog.

4. RESULTS

4.1. Host-Galaxy Σ_M and Σ_{SFR}

In Figures 1 and 2, we plot galaxy stellar-mass density Σ_M and star-formation density Σ_{SFR} , estimated from broadband magnitudes, against stellar mass M . These show that $z < 0.2$ SN Ic-BL and $z < 1.2$ LGRB host galaxies have high stellar-mass density and star-formation density for their stellar masses, compared with the low-redshift ($z < 0.2$) SDSS star-forming galaxy population. In contrast, SN Ib/Ic (with slower ejecta speeds) and SN II show no preference for galaxies that have high stellar-mass density or high star-formation density for their stellar masses.

We compute the residuals of each host galaxy from the SDSS M - Σ_M and M - Σ_{SFR} relations. Our statistical method is to determine the probability that each pair of residual distributions is identical using the Kolmogorov-Smirnov (KS) two-sample test. We find significant evidence for differences between the SN Ic-BL ($n = 16$) and the SN II ($n = 251$; 0.03% and 1.7% for Σ_M and Σ_{SFR} , respectively) host distributions. Comparison between the SN Ic-BL and SN Ib/Ic ($n = 52$) host distributions likewise finds evidence for distinct underlying distributions (0.03% and 5.6%).

The residuals of LGRB ($n = 14$) host galaxies from the SDSS M - Σ_M and M - Σ_{SFR} relations are more positive than (i.e., Σ_M and Σ_{SFR} are greater than) those of SN Ib/Ic (0.1% and 0.0006%, respectively) and SN II (0.07% and 0.07%) hosts, while we find no statistically significant difference with the SN Ic-BL host residual distribution (88% and 13%). The galaxy M - Σ_M relation shows no significant change with increasing redshift to $z \approx 1.1$ (e.g., Barden et al. 2005), so comparisons involving the LGRB host M - Σ_M relation should not be strongly affected by evolution in the galaxy population with redshift.

4.2. Preference for Overdense Galaxies

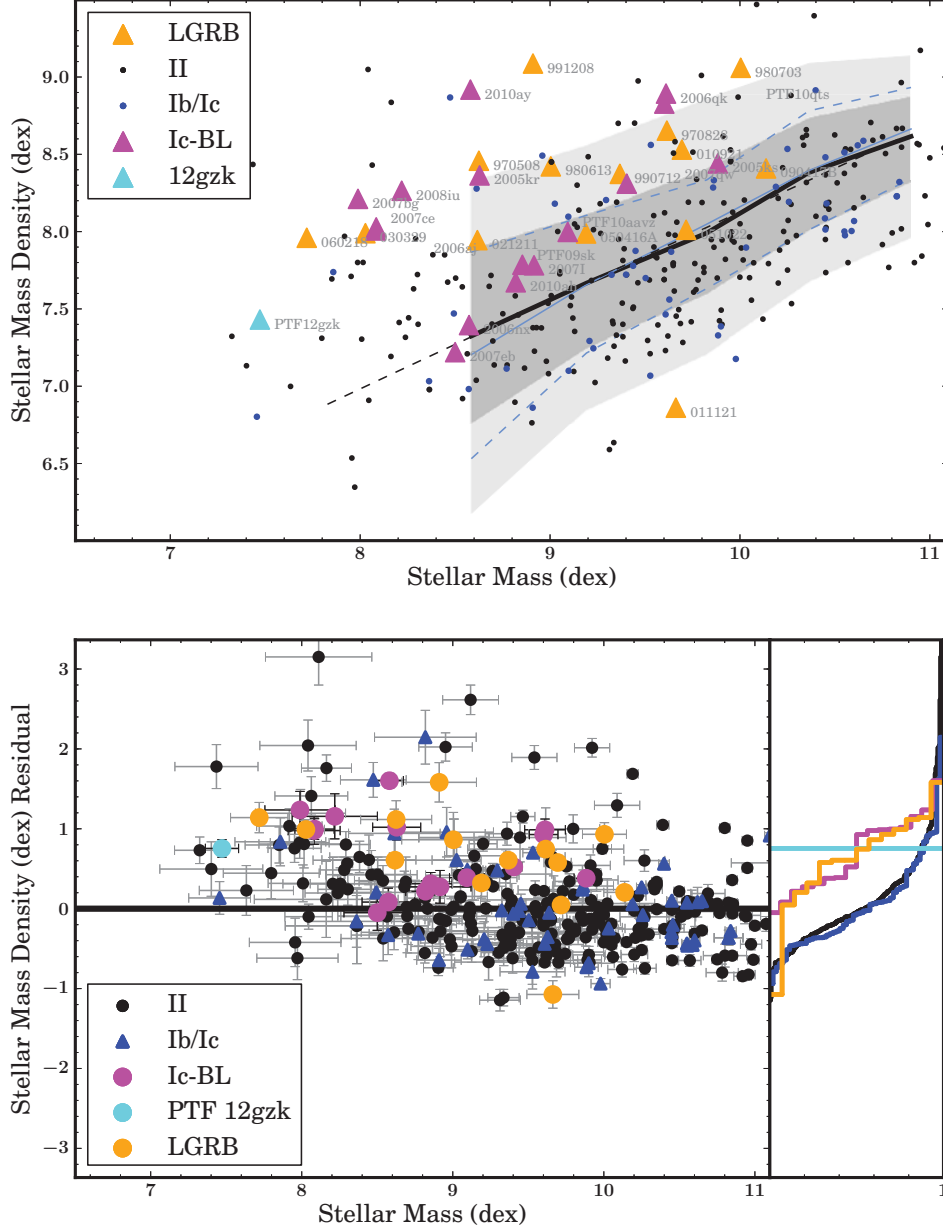


FIG. 1.— Stellar mass density (Σ_M) against host stellar mass for $z < 0.2$ core-collapse SN as well as $z < 1.2$ LGRBs. The host galaxies of broad-lined SN Ic and LGRBs show higher Σ_M for their stellar masses. In the upper panel, the solid black line (median), dark-grey region (68%), and light-grey region (95%) show the distribution of SDSS star-forming galaxies. The blue solid (median) and dashed (68%) lines show the distribution expected for a transient population that follows the SFR. The black dashed line shows the second-order polynomial fit to the median SDSS M - Σ_M relation used to compute a Σ_M residual for each galaxy. Broad features were not evident in the optical spectrum of PTF12gzk, a peculiar SN Ic, but radio observations show evidence for ejecta speeds that reach $\sim 0.3c$ (Horesh et al. 2013). In the lower panel, we plot the residuals of host-galaxy Σ_M from the SDSS M - Σ_M relation, and the cumulative distribution for each host-galaxy sample.

We study the $z < 0.2$ SDSS star-forming population to investigate whether galaxies with relatively high stellar-mass and star-formation densities have comparatively low chemical abundances. In Figure 3, we show the average Tremonti et al. (2004) oxygen abundance of $z < 0.2$ SDSS star-forming galaxies as a function of M and Σ_M as well as Σ_{SFR} . The star-forming SDSS galaxies with the highest stellar-mass or star-formation-rate densities (in each stellar-mass bin) are not, on average, comparatively metal poor. The galaxies with the highest stellar-mass densities are, on average, more metal-rich by ~ 0.2 dex.

An important question is whether the high stellar-mass and

star-formation-rate densities of SN Ic-BL and $z < 1.2$ LGRB host galaxies can be attributed entirely to the preference for low metal abundance observed among low-redshift SN Ic-BL (Kelly & Kirshner 2012; Sanders et al. 2012) and LGRBs (Modjaz et al. 2008; Graham & Fruchter 2013). We can represent such a preference as a progenitor formation efficiency η per unit stellar mass created that depends solely on metallicity Z and diminishes with increasing Z . If η is a function of only metallicity Z , then the rate r of fast-ejecta transients in a galaxy with a given SFR is

$$r \propto \eta(Z) \times \text{SFR}. \quad (5)$$

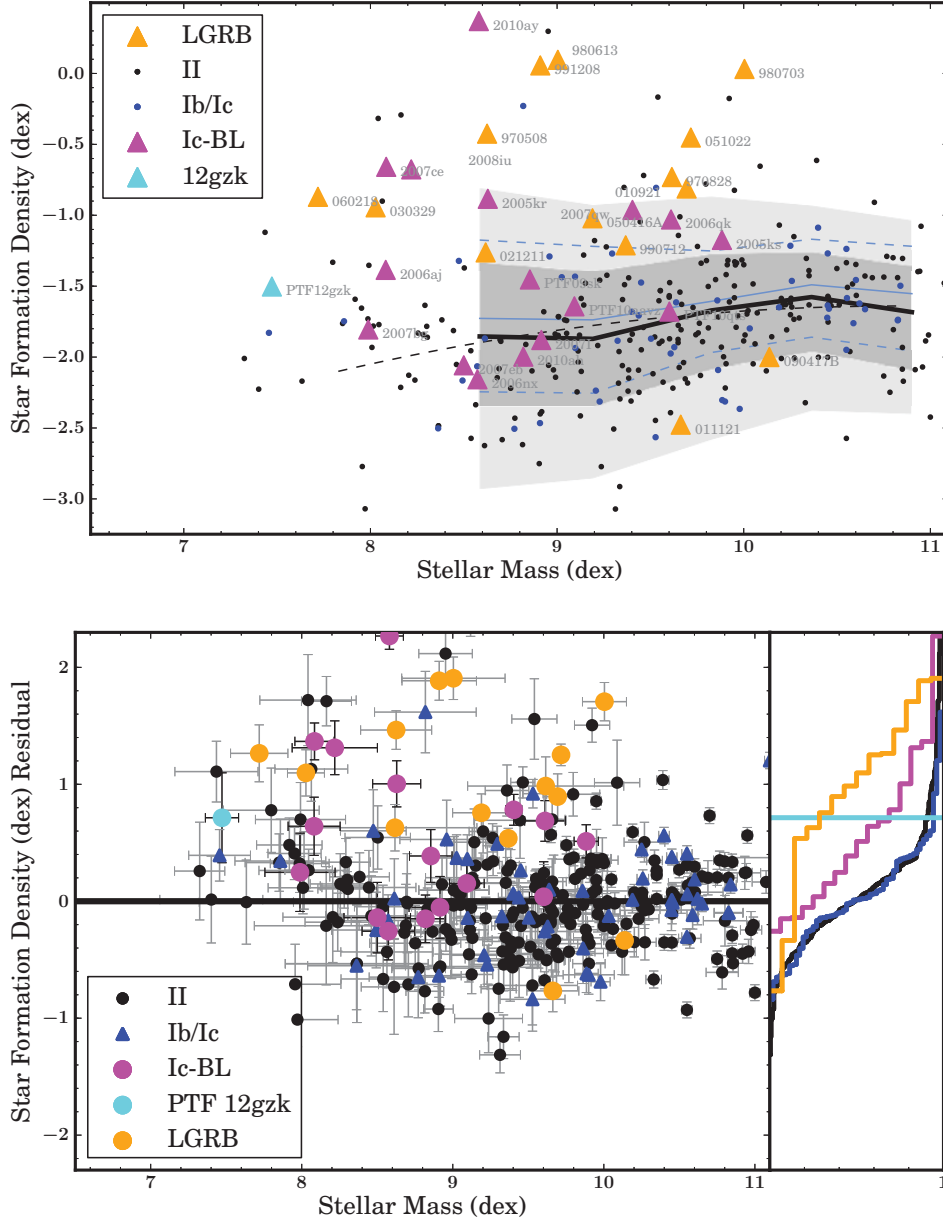


FIG. 2.— As in Figure 1, but showing the star-formation density (Σ_{SFR}) against host stellar mass for $z < 0.2$ core-collapse SN as well as $z < 1.2$ LGRBs. Host galaxies of broad-lined SN Ic and LGRBs show high star-formation densities for their stellar masses.

Half of the star formation in each galaxy mass M bin plotted in Figure 3 occurs in galaxies below the $M - \Sigma_M$ and $M - \Sigma_{\text{SFR}}$ relations marked by thick blue lines. A transient population whose η has no environmental dependence would be expected to explode equally in galaxies above and below these SFR-weighted relations. If η instead increases at low abundance (and depends only on Z), we would expect greater numbers of SN Ic-BL and $z < 1.2$ LGRBs on the side of the relation, either above or below, that is comparatively metal poor.

Inspection of Figure 3 shows that, on average, higher stellar-mass density corresponds to higher metallicity, while metallicity does not vary strongly with star-formation density among galaxies in each bin in stellar mass. Consequently, if η increases at low abundance (and depends only on Z), we would expect a plurality of SN Ic-BL and $z < 1.2$ LGRBs to be below the SFR-weighted $M - \Sigma_M$ relation, and approx-

imately equal numbers above and below the SFR-weighted $M - \Sigma_{\text{SFR}}$ relation. Since this prediction is very different from the pattern we observe, the production of SN Ic-BL and LGRB progenitors much be enhanced by an additional factor other than low metallicity that varies with Σ_M as well as Σ_{SFR} .

4.3. Host-Galaxy Gaseous Velocity Dispersions

High gas dispersion velocities provide additional, independent evidence for distinct physical conditions in the host galaxies of low-redshift SN Ic-BL. In Figure 4, the SN Ic-BL hosts describe an $M - \sigma_{\text{gas}}$ relation with an offset to high gas velocity dispersion measured from the $\text{H}\alpha$ emission lines in the SDSS fiber spectra. The SN Ic-BL host distribution is significantly different from the SN Ib/Ic (0.6%) and the SN II (0.02%) host distributions.

The comparatively high gas velocity dispersions of SN Ic-

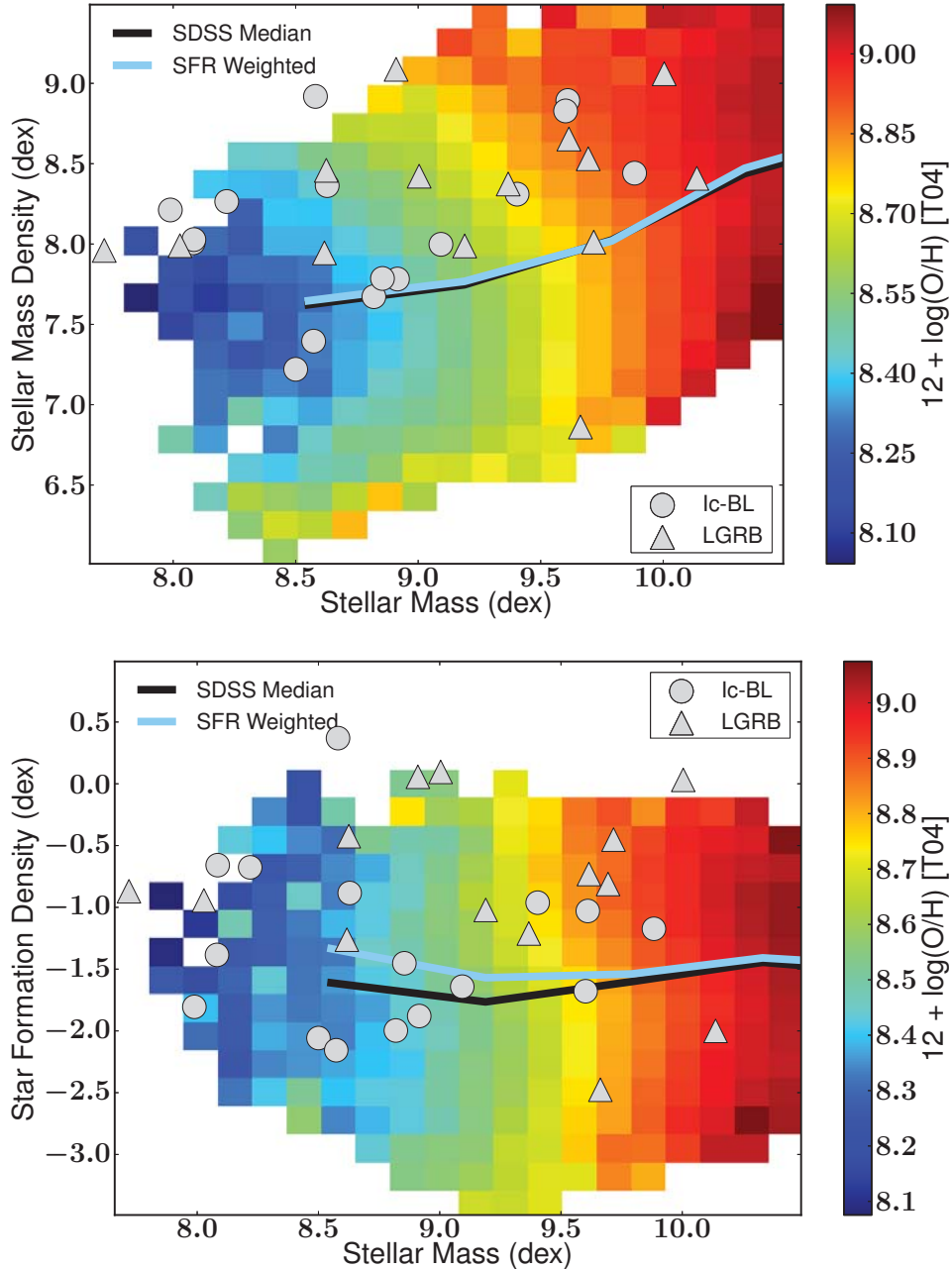


FIG. 3.— Variation in mean SDSS oxygen abundance as a function of galaxy stellar mass (M) and stellar-mass density (Σ_M) as well as star-formation density (Σ_{SFR}). The host galaxies of nearby SN Ic-BL (grey circles) and $z < 1.2$ LGRBs (grey triangles) are overlotted. Among galaxies with masses typical of those of SN Ic-BL and LGRB hosts ($\lesssim 10^{10} M_\odot$), galaxies with high Σ_M have (on average) modestly higher abundances, while those with high Σ_{SFR} are at least as metal-rich as those with low Σ_{SFR} . Solid black and blue lines are as in Figure 1. If the production SN Ic-BL and LGRB progenitors depended only on metallicity (and increased at low abundance), we would expect them to occur more frequently among the metal-poor galaxies below the blue SFR-weighted $M - \Sigma_M$ relation, and approximately equally above and below the blue SFR-weighted $M - \Sigma_{\text{SFR}}$ relation. Since their actual distribution differs strongly from this prediction, this suggests that the SN Ic-BL and LGRB rate is enhanced by a factor other than low metal abundance that varies with Σ_M and Σ_{SFR} . An average number of 520 SDSS galaxies populate each plotted bin, and the average uncertainty of the mean abundance is 0.022 dex. Average uncertainties of plotted SN Ic-BL and LGRB host galaxy stellar-mass and star-formation-rate densities are 0.18 and 0.19 dex, respectively (see Figures 1 and 2).

BL host galaxies may have one or more physical explanations. Rotationally supported galaxies having more compact and dense mass configurations are expected to have higher velocity dispersions. Alternatively, recent analysis of the gas kinematics of a sample of $z \approx 0.1$ – 0.3 compact, highly star-forming galaxies finds complex profiles for the strong emission lines, with several narrow ($\sigma_{\text{gas}} \approx 10$ – 120 km s^{-1}) and broad ($\sigma_{\text{gas}} \approx 100$ – 250 km s^{-1}) components (Amorín et al. 2012) that may be due to strong stellar winds, or emission

from expanding SN remnants.

In Figures 5 and 6, we show images of core-collapse SN host galaxies and the measured $\text{H}\alpha$ velocity dispersions juxtaposed with control samples of SDSS star-forming galaxies having similar parameters. These demonstrate the high velocity dispersions of SN Ic-BL host galaxies.

4.4. Host-Galaxy Sizes

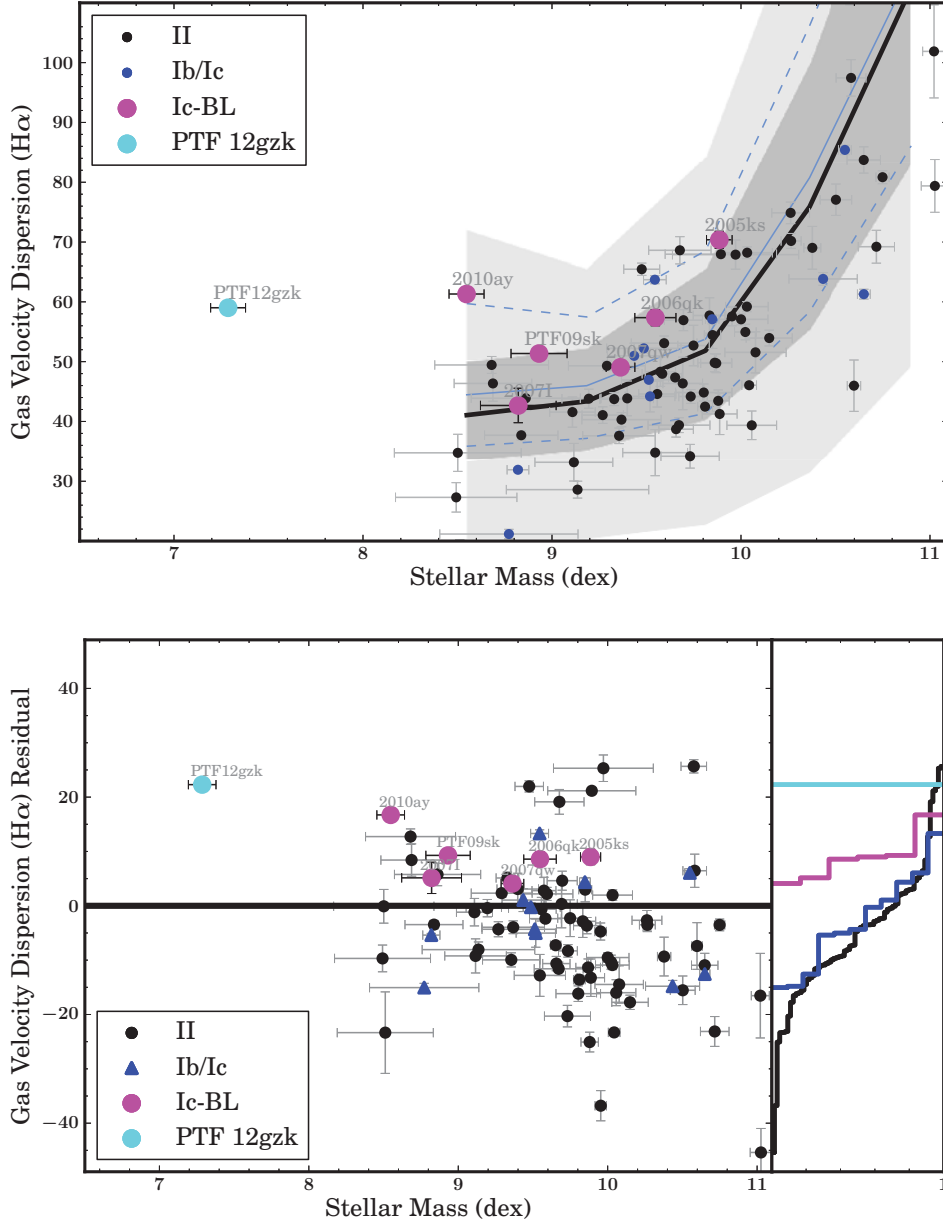


FIG. 4.— Host-galaxy gas velocity dispersion inferred from the $H\alpha$ emission-line profile against host stellar mass. Host galaxies of broad-lined SN Ic (magenta) as well as that of PTF12gzk show high gas velocity dispersion. Residuals plotted below are from the values predicted from locally weighted linear least-squares fits performed on the SDSS catalog. At bottom right, we show the cumulative distribution for each SN sample.

In Figures 7 and 8, we plot galaxy half-light radius r_{50} (in kpc) against M and SFR estimated from their broadband magnitudes. These show that $z < 0.2$ SN Ic-BL and $z < 1.2$ LGRB host galaxies are compact for their stellar masses and SFRs, compared with the low-redshift ($z < 0.2$) SDSS star-forming galaxy population. In contrast, SN Ib/Ic (with slower ejecta speeds) and SN II show no preference for galaxies that are relatively compact in size.

4.5. Hybrid Σ_{SFR} Estimates

In Figure 9, we plot Σ_{SFR} against M for the sample of nearby ($z < 0.2$) core-collapse SN galaxies with SDSS spectra. Here we calculate Σ_{SFR} using the SFR estimated by the MPA-JHU group from the fiber spectrum and by modeling the galaxy *ugriz* light outside of the $3''$ fiber. These SFR measurements may be expected to be more accurate and precise

than the SFR estimates that are based on galaxy broadband photometry alone, and provide evidence that the preference among SN Ic-BL and LGRBs for high Σ_{SFR} seen in Figure 2 galaxies is robust. The SN Ic-BL ($n = 6$) and SN II ($n = 70$) distributions show significantly different ($p = 3.2\%$) residual distributions from their predicted Σ_{SFR} values.

4.6. M -SFR Relation

Figure 10 shows the relationship between M and SFR for the core-collapse host galaxies and the SDSS star-forming population. This shows that host galaxies of SN Ic-BL are not substantially more strongly star forming for their stellar masses than other core-collapse hosts, and suggests that relatively compact host sizes may primarily account for their high star-formation-rate densities.



FIG. 5.— Comparison between the host galaxies of broad-lined SN Ic and SDSS galaxies with similar redshift z , stellar mass M , and ellipticity ϵ . Each row, ordered according the gaseous velocity dispersion estimated from the $H\alpha$ emission line, shows the host galaxy of a broad-lined SN Ic and the six nearest neighbors in the vector space $\mathbf{x} = (\log_{10}(M/0.1), z/0.01, \epsilon/0.05)$. These comparisons show that the host galaxies of broad-lined SN Ic have comparatively high velocity dispersions for their host-galaxy stellar masses. Red circles represent the 3'' SDSS fiber aperture, while the white squares are positioned at the location of the SN explosion. From the top to the bottom row, host galaxies are those of SN 2007I, SN 2007qw, SN 2005ks, SN 2006qk, PTF 09sk, and SN 2010ay.

4.7. $M-Z$ Relation

Given the existing evidence that $z \lesssim 0.3$ SN Ic-BL (Kelly & Kirshner 2012; Sanders et al. 2012) and LGRBs (Modjaz et al. 2008; Graham & Fruchter 2013) prefer metal-poor environments, a reasonable question is whether the high Σ_M and Σ_{SFR} host galaxies in our sample having SDSS spectra describe a metal-poor mass-metallicity ($M-Z$) relation. Kelly et al. (2014, in prep.) report no significant evidence that the SN Ic-BL offset distribution ($n = 6$) differs from the SN Ib/Ic (65%; $n = 11$) or the SN II (19%; $n = 59$) distributions.

5. DISCUSSION

We have found that low-redshift SN Ic-BL and $z < 1.2$ LGRB host galaxies show stellar-mass and star-formation densities high compared with those of low-redshift galaxies having similar stellar masses. Core-collapse SN with more slowly expanding ejecta, however, exhibit no preference for galaxies having overdense stellar-mass distributions and star formation. SN Ic-BL host galaxies exhibit high gas velocity dispersions for their stellar masses, providing evidence for exceptional conditions in their hosts.

Given the effect of stellar metallicity to strengthen line-driven winds and remove the angular momentum of massive stars, studies of SN and LGRB host galaxies have often attempted to explain environmental patterns in terms of chemical abundance. However, across the stellar-mass range populated by SN Ic-BL and LGRB hosts, SDSS star-forming galaxies with high stellar-mass and star-formation-rate densities are not, on average, more metal poor than less dense galaxies having similar stellar masses (see Figure 3). Therefore, a preference other than for low metallicity environments must be responsible for the overrepresentation of SN and LGRBs in galaxies with high stellar-mass and star-formation-rate densities. Furthermore, the $M-Z$ relation of SN Ic-BL host galaxies, which have high stellar-mass and star-formation densities, is not significantly metal poor compared to the SDSS $M-Z$ relation (Kelly et al. 2014, in prep.).

In fact, a preference of high-velocity explosions for rapidly star-forming or overdense regions may help explain the observed association of LGRBs with the brightest regions of their host galaxies (Fruchter et al. 2006). An initial suggestion was that a strong association with the brightest regions would

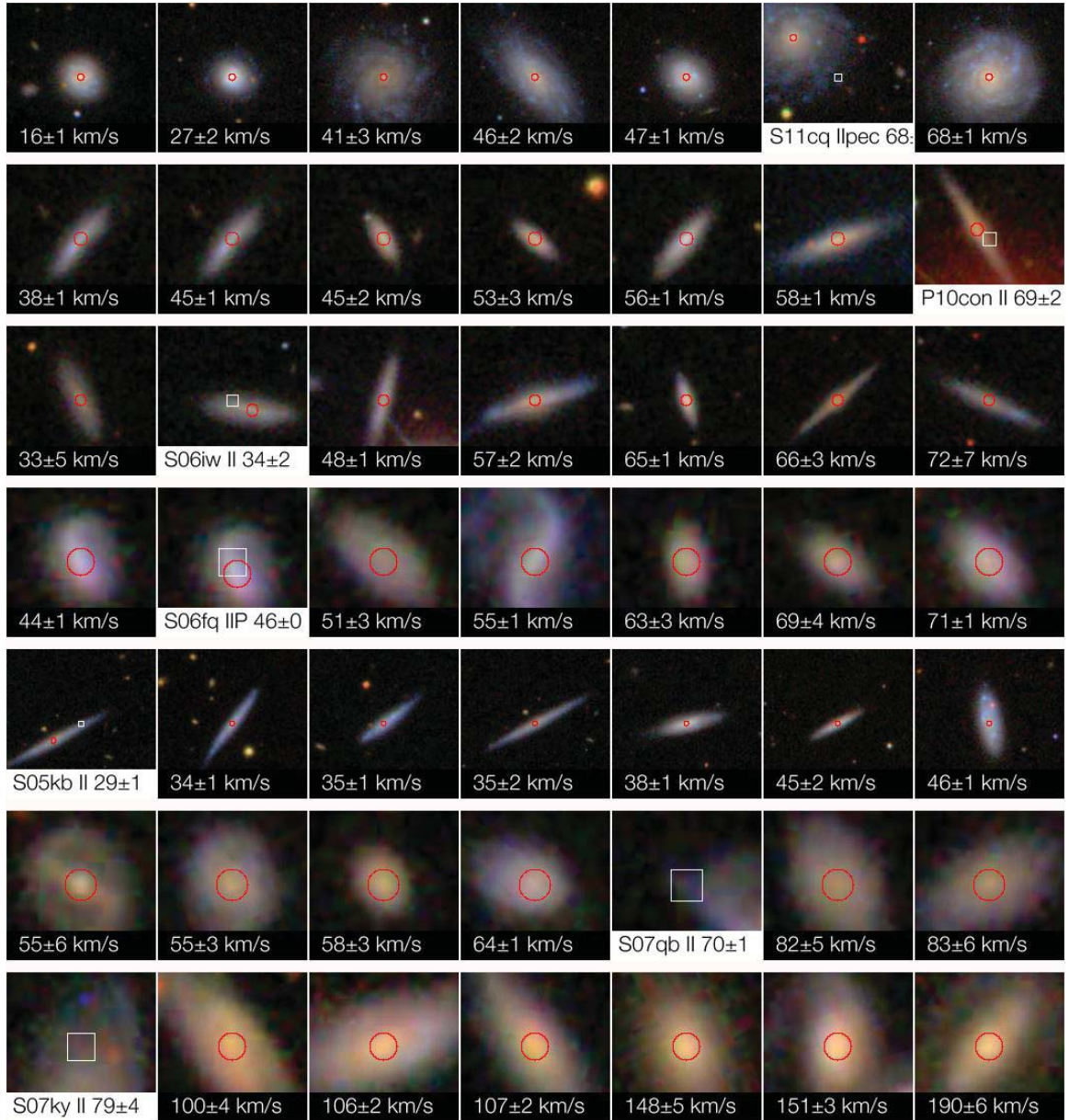


FIG. 6.— Same as Figure 5, but for SN II host galaxies. In contrast to the hosts of SN Ic-BL, the host galaxies of SN II have σ_{vel} measurements that are both low and high in comparison to galaxies having similar redshift z , stellar mass M , and ellipticity ϵ . From the top to the bottom row, host galaxies are those of SN 2011cq, PTF 10con, SN 2006iw, SN 2006fq, SN 2005kb, SN 2007qb, and SN 2007ky.

be expected for LGRBs if they occur preferentially in low-mass, metal-poor galaxies. If the most massive stars form in OB associations, then these will be more likely to correspond to the peaks of the light distribution of low-mass, metal-poor galaxies. OB associations in more massive, metal-rich spirals may instead be outranked in brightness by, for example, the nucleus. While such a low-metallicity preference may contribute, we suggest that an affinity to high star-formation density is important.

A plausible explanation for the association of LGRBs with regions of higher star-formation density is the formation efficiency of young, bound star clusters. Observations of extragalactic star clusters have found evidence that bound-cluster formation efficiency increases with the star-formation density (Goddard et al. 2010; Silva-Villa et al. 2013). Binary systems may be created more frequently in bound clusters, and

those that form are expected to become progressively tighter through dynamical interactions with other members of the cluster (Heggie 1975; Hut et al. 1992). Therefore, massive stars that form in dense star clusters are more likely to be in tight binary systems. Interacting massive binaries are candidate progenitor systems for SN Ic-BL and LGRBs, because mass transfer or common-envelope evolution leading (in some cases) to a merger can yield a rapidly rotating star whose outer envelope is not composed of H.

If SN Ic-BL and LGRBs explode from stars that are more massive than the progenitors of SN Ib/Ic and SN II, an IMF that becomes top-heavy in dense, highly star-forming regions provides an alternative explanation for the patterns we observe. Indirect evidence from the absorption features of $\lesssim 0.3 M_{\odot}$ stars suggests instead that the IMF may be bottom-heavy in elliptical galaxies with high stellar velocity dis-

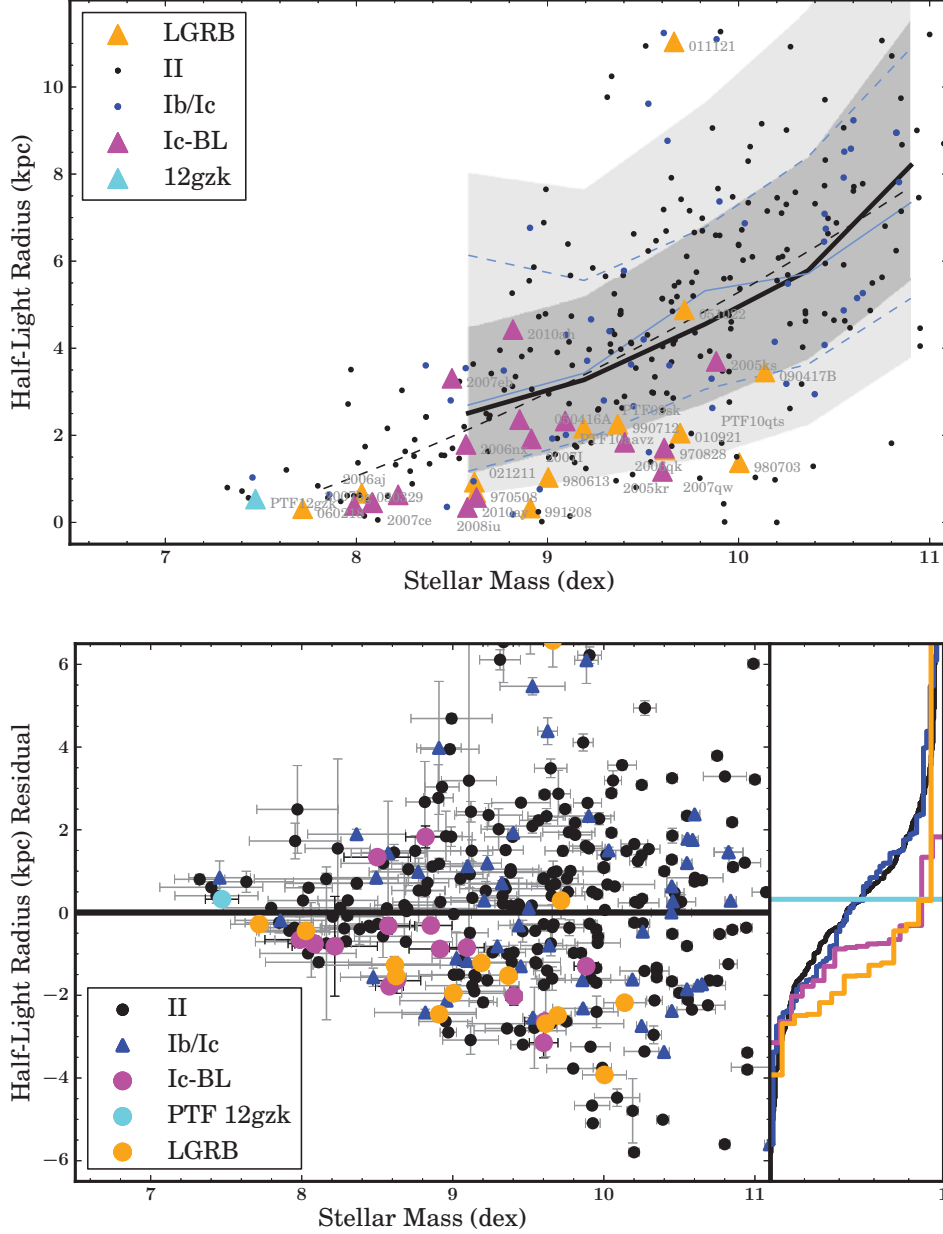


FIG. 7.— As in Figure 1, but showing the effective host-galaxy radius (r_{50}) against host SFR for $z < 0.2$ core-collapse SN as well as $z < 1.2$ LGRBs. Host galaxies of broad-lined SN Ic and LGRBs are compact for their stellar masses.

persions and $[\text{Mg}/\text{Fe}]$, which are thought to have had high star formation densities during their formation epoch (van Dokkum & Conroy 2010; Conroy & van Dokkum 2012). This suggests that the IMF may be bottom heavy in dense, highly star-forming regions, while the opposite trend would be required to explain our observations. An improved census of massive stars across low-redshift environments may help to address more directly whether the patterns we have found can be explained by variation in the upper end of the IMF.

The median redshift ($z_m = 0.55$) of the $z < 1.2$ LGRB sample is substantially higher than those of the core-collapse SN sample ($z_m \approx 0.07$) and the SDSS sample of galaxy spectra ($z_m \approx 0.08$). The $M-\Sigma_M$ and $M-\Sigma_{\text{SFR}}$ relations among star-forming galaxies may evolve toward lower Σ_M and Σ_{SFR} densities from $z \approx 0.55$ to the low-redshift universe. As we have shown, however, the low-redshift SN Ic-BL host galaxy

population exhibits the same preference for high stellar-mass and star-formation density galaxies as LGRBs. Additionally, if stellar-mass and star-formation-rate density are proxies for the star-forming conditions that promote the formation of SN Ic-BL progenitors, then we expect that these same physical conditions exist in high-redshift LGRB host galaxies having similar positions in the $M-\Sigma_M$ and $M-\Sigma_{\text{SFR}}$ planes.

Given the evidence that the progenitors of high-velocity ejecta core-collapse explosions form more efficiently in galaxies that have high stellar-mass and star-formation densities, a reasonable expectation is that LGRBs will be improved tracers of star formation at earlier epochs where galaxies have higher densities of stellar mass and ongoing star formation than in the low-redshift universe (Trujillo et al. 2006).

LGRBs may be the most powerful probes of star formation at the highest redshifts. The extreme luminosities of LGRBs

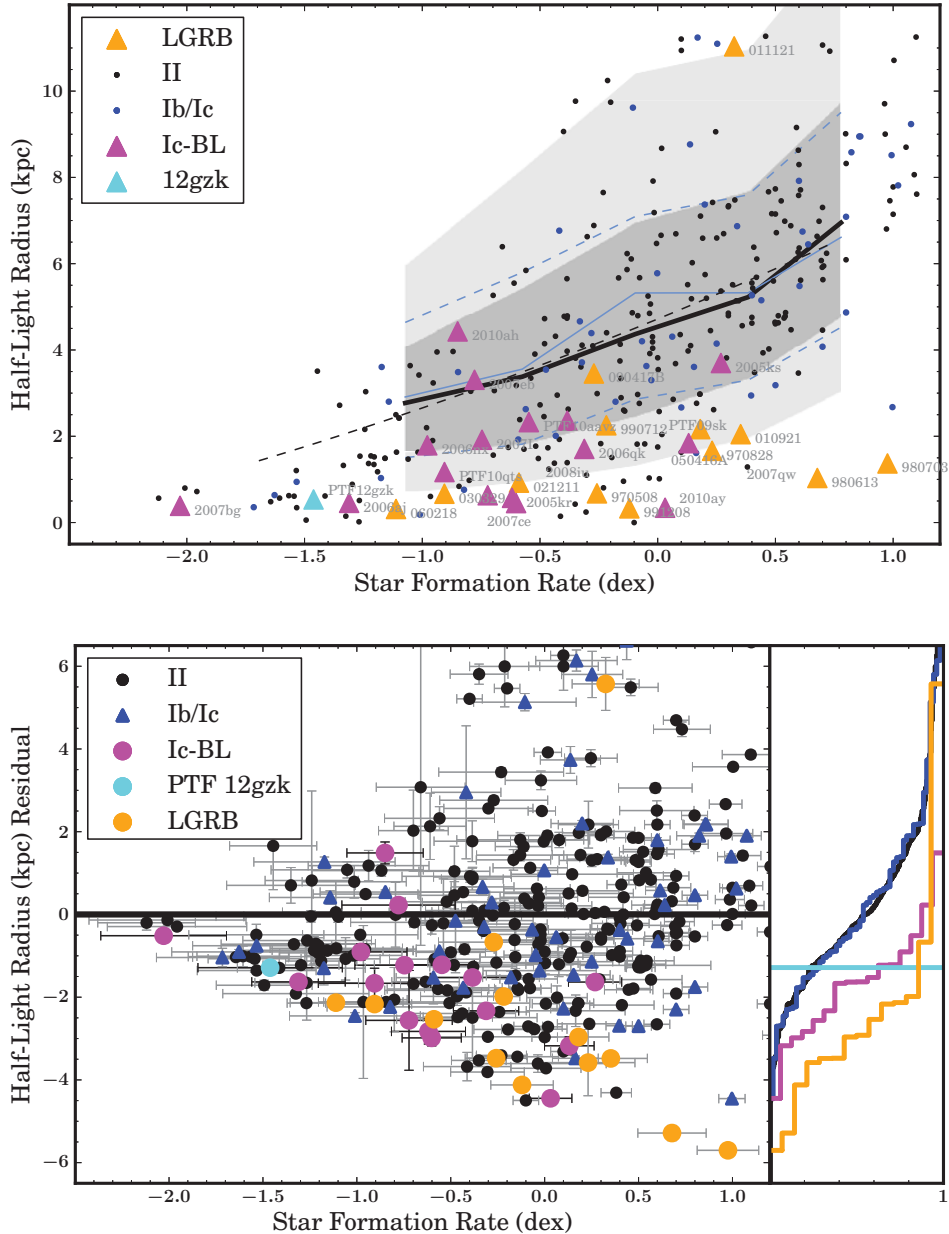


FIG. 8.— As in Figure 1, but showing the effective host-galaxy radius (r_{50}) against host SFR for $z < 0.2$ core-collapse SN as well as $z < 1.2$ LGRBs. Host galaxies of broad-lined SN Ic and LGRBs are compact for their SFR.

allow detection at the earliest epochs of star formation ($z \gtrsim 8$), where optical and infrared instruments are not yet able to detect sub- L_* galaxies. The evidence we have found that the formation of LGRB progenitors depends sensitively on star-forming conditions early star formation in detail.

6. CONCLUSIONS

We have studied the host galaxies of a sample of 245 low-redshift core-collapse SN, including 17 SN Ic-BL discovered by galaxy-untargeted searches and 15 optically luminous and dust-obscured $z < 1.2$ LGRBs. We have used the uniform fiber spectra and photometry of the SDSS to measure the properties of the core-collapse SN host-galaxy sample, as well as characterize the low-redshift star-forming galaxy population. Published multi-band photometry as well as *HST* imag-

ing were used to study the $z < 1.2$ LGRB host galaxies.

The outflowing ejecta of SN Ic-BL, from the wide features of their spectra, and of LGRBs, through their association with SN Ic-BL and γ -ray emission, are inferred to expand with high velocities ($\sim 20,000\text{--}30,000 \text{ km s}^{-1}$). We have found that these core-collapse explosions in which a significant fraction of the ejecta is moving at high velocity prefer galaxies with high stellar-mass and star-formation densities, when compared to galaxies having similar stellar masses. The core-collapse SN in our sample having typical velocities of their ejecta, in contrast, are found approximately equally in galaxies with comparatively low and high stellar-mass and star-formation densities. From the widths of $H\alpha$ emission lines, we find that the hosts of SN Ic-BL have exceptionally high gas velocity dispersions when compared with star-forming galaxies having similar stellar masses.

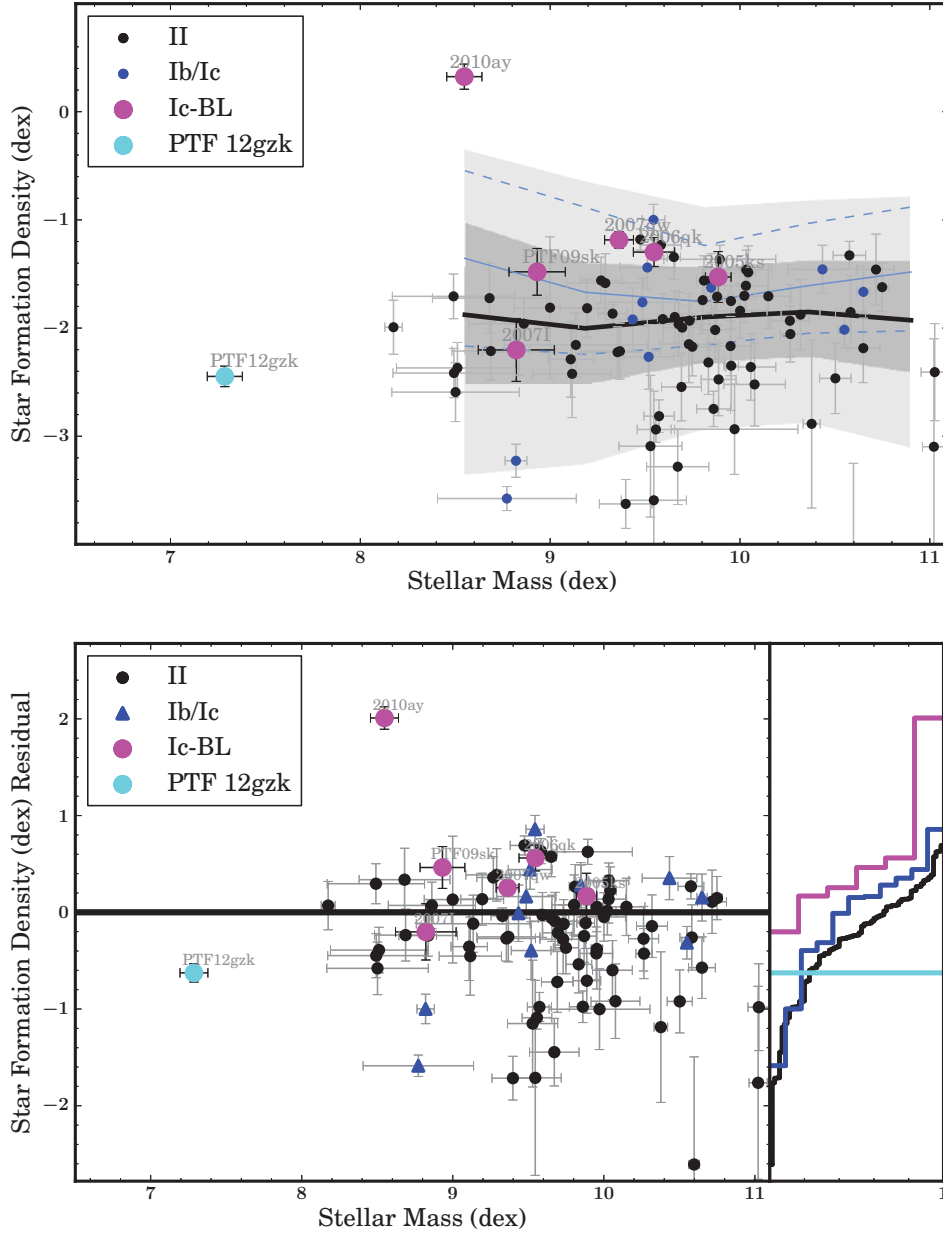


FIG. 9.— As in Figure 1, but showing host galaxy hybrid spectroscopic star-formation density against stellar mass. The star-formation density Σ_{SFR} plotted here is calculated using an SFR estimate using the SDSS fiber spectrum and by modeling the host light outside of the $3''$ fiber. The SN Ic-BL host galaxies show high Σ_{SFR} for their stellar masses, which is consistent with the pattern observed with Σ_{SFR} estimated from photometry alone.

While early LGRB host environment analyses helped to establish the connection between LGRBs and massive stars (e.g., Bloom et al. 2002), subsequent analysis has focused on the effect of metal abundance on the creation of their progenitors (e.g., Modjaz et al. 2008), or sought to explain environmental patterns in terms of a preference for metal-poor galaxies (e.g., Fruchter et al. 2006; Svensson et al. 2010; Graham & Fruchter 2013). Here we have shown that the preference of low-redshift SN Ic-BL and $z < 1.2$ LGRBs for galaxies with high stellar-mass and star-formation-rate densities, compared to star-forming galaxies of similar stellar mass, is separate from a preference for low metal abundances.

Observations of extragalactic star formation have suggested that dense stellar clusters may form with greater efficiency in regions of dense star formation (Goddard et al. 2010; Silva-Villa et al. 2013). A prospective explanation for the host-galaxy patterns we find is the efficient formation of tight massive binary progenitor systems in such densely star-forming environments. Alternatively, if SN Ic-BL and LGRB progenitors have greater stellar masses than those of core-collapse SN with typical ejecta velocities, a top-heavy IMF in galaxies with high stellar-mass density and star-formation density could account for these same patterns. However, such a top-heavy IMF would need to be reconciled with evidence instead for a bottom-heavy IMF in massive galaxies that were densely star forming while assembling their mass (van Dokkum &

Conroy 2010; Conroy & van Dokkum 2012). The construction of ground-based telescopes with large aperture (e.g., the Thirty Meter Telescope; Giant Magellan Telescope) and the James Webb Space Telescope will make possible observations of galaxies formed shortly after reionization, but the faintest galaxies will remain beyond their sensitivity. LGRBs, whose γ -ray emission is currently visible to $z \approx 8$ (Tanvir et al. 2009), may provide an effective approach to probing the detailed star-forming conditions in these early galaxies.

We thank Sandra Savaglio who, as referee, provided insightful comments and suggestions. We additionally acknowledge useful discussions about measurements and host galaxies with Jarle Brinchmann, Ori Fox, David Elbaz, John Graham, Matt Lehnert, Steven Stahler, Paul Crowther, and Josh Bloom. A.V.F.'s group at UC Berkeley has received generous financial assistance from the Christopher R. Redlich Fund, the TABASGO Foundation, Weldon Wood, and NSF grant AST-1211916, as well as from NASA/*HST* grant AR-12850 from the Space Telescope Science Institute, which is operated by the Association of Universities for Research in Astronomy (AURA), Inc., under NASA contract NAS5-26555. This research has made use of the GHostS database (www.grbhosts.org), which is partly funded by NASA/*Spitzer* RSA Agreement No. 1287913.

REFERENCES

- Ahn, C. P., Alexandroff, R., Allende Prieto, C., et al. 2013, ArXiv e-prints
 Amorín, R., Vilchez, J. M., Hägele, G. F., et al. 2012, *ApJ*, 754, L22
 Arcavi, I., Gal-Yam, A., Kasliwal, M. M., et al. 2010, *ApJ*, 721, 777
 Baldry, I. K., Glazebrook, K., Budavári, T., et al. 2005, *MNRAS*, 358, 441
 Baldwin, J. A., Phillips, M. M., & Terlevich, R. 1981, *PASP*, 93, 5
 Barden, M., Rix, H.-W., Somerville, R. S., et al. 2005, *ApJ*, 635, 959
 Ben-Ami, S., Gal-Yam, A., Filippenko, A. V., et al. 2012, *ApJ*, 760, L33
 Bertin, E., & Arnouts, S. 1996, *AJ*, 117, 393
 Bloom, J. S., Kulkarni, S. R., & Djorgovski, S. G. 2002, *AJ*, 123, 1111
 Cappellari, M., & Emsellem, E. 2004, *PASP*, 116, 138
 Cenko, S. B., Kelemen, J., Harrison, F. A., et al. 2009, *ApJ*, 693, 1484
 Conroy, C., & van Dokkum, P. G. 2012, *ApJ*, 760, 71
 Conselice, C. J., Vreeswijk, P. M., Fruchter, A. S., et al. 2005, *ApJ*, 633, 29
 Djorgovski, S. G., Frail, D. A., Kulkarni, S. R., et al. 2001, *ApJ*, 562, 654
 Elliott, J., Krühler, T., Greiner, J., et al. 2013, *A&A*, 556, A23
 Filippenko, A. V. 1997, *ARA&A*, 35, 309
 Fioc, M., & Rocca-Volmerange, B. 1999, ArXiv e-prints
 Fruchter, A. S., Levan, A. J., Strolger, L., et al. 2006, *Nature*, 441, 463
 Galama, T. J., Vreeswijk, P. M., van Paradijs, J., et al. 1998, *Nature*, 395, 670
 Goddard, Q. E., Bastian, N., & Kennicutt, R. C. 2010, *MNRAS*, 405, 857
 Graham, J. F., & Fruchter, A. S. 2013, *ApJ*, 774, 119
 Heggie, D. C. 1975, *MNRAS*, 173, 729
 Hirschi, R., Meynet, G., & Maeder, A. 2005, *A&A*, 443, 581
 Hjorth, J., Sollerman, J., Møller, P., et al. 2003, *Nature*, 423, 847
 Horesh, A., Kulkarni, S. R., Corsi, A., et al. 2013, ArXiv e-prints, arXiv:1306.5755
 Hut, P., McMillan, S., Goodman, J., et al. 1992, *PASP*, 104, 981
 Kelly, P. L., Filippenko, A. V., Fox, O. D., Zheng, W., & Clubb, K. I. 2013, *ApJ*, 775, L5
 Kelly, P. L., Hicken, M., Burke, D. L., Mandel, K. S., & Kirshner, R. P. 2010, *ApJ*, 715, 743
 Kelly, P. L., & Kirshner, R. P. 2012, *ApJ*, 759, 107
 Kelly, P. L., Kirshner, R. P., & Pahre, M. 2008, *ApJ*, 687, 1201
 Klose, S., Henden, A. A., Greiner, J., et al. 2003, *ApJ*, 592, 1025
 Kocovski, D., West, A. A., & Modjaz, M. 2009, *ApJ*, 702, 377
 Langer, N. 2012, *ARA&A*, 50, 107
 Langer, N., & Norman, C. A. 2006, *ApJ*, 638, L63
 Law, N. M., Kulkarni, S. R., Dekany, R. G., et al. 2009, *PASP*, 121, 1395
 Levesque, E. M., Kewley, L. J., Graham, J. F., & Fruchter, A. S. 2010, *ApJ*, 712, L26
 Li, W., Leaman, J., Chornock, R., et al. 2011, *MNRAS*, 412, 1441
 MacFadyen, A. I., & Woosley, S. E. 1999, *ApJ*, 524, 262
 Matheson, T., Garnavich, P. M., Stanek, K. Z., et al. 2003, *ApJ*, 599, 394
 Modjaz, M. 2011, *Astronomische Nachrichten*, 332, 434
 Modjaz, M., Kewley, L., Kirshner, R. P., et al. 2008, *AJ*, 135, 1136
 Peng, C. Y., Ho, L. C., Impey, C. D., & Rix, H.-W. 2002, *AJ*, 124, 266
 Perley, D. A., Cenko, S. B., Bloom, J. S., et al. 2009, *AJ*, 138, 1690
 Perley, D. A., Levan, A. J., Tanvir, N. R., et al. 2013, ArXiv e-prints, arXiv:1301.5903
 Petrosian, V. 1976, *ApJ*, 209, L1
 Podsiadlowski, P., Ivanova, N., Justham, S., & Rappaport, S. 2010, *MNRAS*, 406, 840
 Prochaska, J. X., Chen, H.-W., Dessauges-Zavadsky, M., & Bloom, J. S. 2007, *ApJ*, 666, 267
 Rau, A., Kulkarni, S. R., Law, N. M., et al. 2009, *PASP*, 121, 1334
 Sana, H., de Mink, S. E., de Koter, A., et al. 2012, *Science*, 337, 444
 Sanders, N. E., Soderberg, A. M., Levesque, E. M., et al. 2012, *ApJ*, 758, 132
 Sarzi, M., Falcón-Barroso, J., Davies, R. L., et al. 2006, *MNRAS*, 366, 1151
 Savaglio, S., Glazebrook, K., & Le Borgne, D. 2009, *ApJ*, 691, 182
 Savaglio, S., Rau, A., Greiner, J., et al. 2012, *MNRAS*, 420, 627
 Silva-Villa, E., Adamo, A., & Bastian, N. 2013, ArXiv e-prints
 Singer, L. P., Cenko, S. B., Kasliwal, M. M., et al. 2013, *ApJ*, 776, L34
 Smartt, S. J., Eldridge, J. J., Crockett, R. M., & Maund, J. R. 2009, *MNRAS*, 395, 1409
 Stanek, K. Z., Matheson, T., Garnavich, P. M., et al. 2003, *ApJ*, 591, L17
 Strauss, M. A., Weinberg, D. H., Lupton, R. H., et al. 2002, *AJ*, 124, 1810
 Svensson, K. M., Levan, A. J., Tanvir, N. R., Fruchter, A. S., & Strolger, L.-G. 2010, *MNRAS*, 405, 57
 Tanvir, N. R., Fox, D. B., Levan, A. J., et al. 2009, *Nature*, 461, 1254
 Taylor, G. B., Frail, D. A., Kulkarni, S. R., et al. 1998, *ApJ*, 502, L115
 Thomas, D., Steele, O., Maraston, C., et al. 2013, *MNRAS*, 431, 1383
 Tremonti, C. A., Heckman, T. M., Kauffmann, G., et al. 2004, *ApJ*, 613, 898
 Trujillo, I., Förster Schreiber, N. M., Rudnick, G., et al. 2006, *ApJ*, 650, 18
 van Dokkum, P. G., & Conroy, C. 2010, *Nature*, 468, 940
 Vink, J. S., de Koter, A., & Lamers, H. J. G. L. M. 2001, *A&A*, 369, 574
 Woosley, S. E., & Bloom, J. S. 2006, *ARA&A*, 44, 507
 Woosley, S. E., & Heger, A. 2006, *ApJ*, 637, 914
 Woosley, S. E., Langer, N., & Weaver, T. A. 1993, *ApJ*, 411, 823
 Yoon, S., & Langer, N. 2005, *A&A*, 443, 643

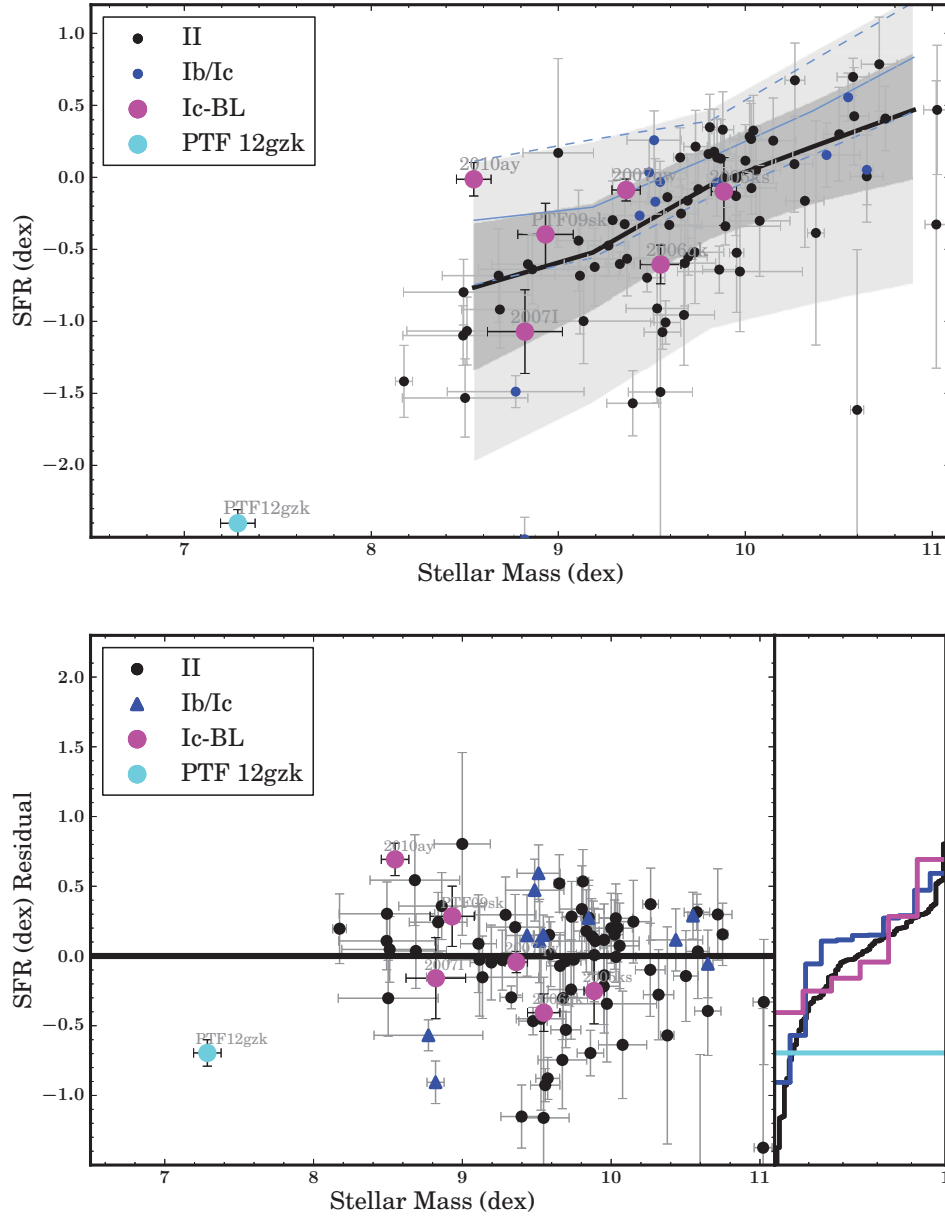


FIG. 10.— As in Figure 1, but showing SFR against host stellar mass for $z < 0.2$ core-collapse SN. The host galaxies of SN Ic-BL exhibit an approximate agreement with the SDSS M -SFR relation.

TABLE 2
 PROPERTIES OF HOST GALAXIES FROM PHOTOMETRY AND IMAGING

Name	z	Type	Mass ($\log M_{\odot}$)	SFR (phot) ($\log M_{\odot} \text{ yr}^{-1}$)	Σ_M ($\log M_{\odot} \text{ kpc}^{-2}$)	Σ_{SFR} ($\log M_{\odot} \text{ yr}^{-1} \text{ kpc}^{-2}$)	r_{50} (kpc)
GRB010921	0.451	GRB	9.69±0.09	0.35±0.19	8.53±0.09	-0.81±0.19	2.05±0.02
GRB011121	0.362	GRB	9.66±0.17	0.32±0.18	6.86±0.17	-2.48±0.18	11.04±0.64
GRB021211	1.006	GRB	8.62±0.54	-0.59±0.20	7.94±0.54	-1.26±0.20	0.93±0.02
GRB030329	0.168	GRB	8.03±0.12	-0.91±0.20	7.99±0.12	-0.94±0.20	0.67±0.03
GRB050416A	0.653	GRB	9.19±0.19	0.18±0.16	7.99±0.19	-1.02±0.16	2.17±0.12
GRB051022	0.807	GRB	9.72±0.05	1.25±0.09	8.01±0.05	-0.45±0.09	4.88±0.44
GRB060218	0.034	GRB	7.72±0.19	-1.11±0.24	7.96±0.19	-0.87±0.24	0.31±0.00
GRB090417B	0.345	GRB	10.14±0.14	-0.27±0.29	8.41±0.14	-2.00±0.29	3.45±0.06
GRB970508	0.835	GRB	8.62±0.24	-0.26±0.17	8.46±0.24	-0.42±0.17	0.68±0.01
GRB970828	0.960	GRB	9.62±0.52	0.23±0.25	8.65±0.52	-0.73±0.25	1.66±0.80
GRB980613	1.097	GRB	9.00±0.34	0.68±0.18	8.42±0.34	0.10±0.18	1.03±0.19
GRB980703	0.966	GRB	10.00±0.15	0.98±0.16	9.06±0.15	0.03±0.16	1.37±0.04
GRB990712	0.433	GRB	9.37±0.05	-0.22±0.09	8.37±0.05	-1.21±0.09	2.25±0.08
GRB991208	0.706	GRB	8.91±0.25	-0.12±0.17	9.09±0.25	0.06±0.17	0.33±0.02
PTF 09awk	0.062	Ib	9.53±0.07	0.16±0.12	8.56±0.07	-0.81±0.12	1.61±0.05
PTF 09axc	0.115	II	9.99±0.06	-0.19±0.18	8.87±0.06	-1.32±0.18	1.51±0.07
PTF 09axi	0.064	II	9.33±0.09	-0.28±0.15	7.42±0.09	-2.18±0.15	4.10±0.15
PTF 09bce	0.023	II	10.95±0.03	0.70±0.07	9.17±0.03	-1.08±0.07	4.46±0.03
PTF 09bw	0.150	II	9.55±0.17	-0.26±0.36	7.90±0.17	-1.90±0.36	2.99±0.40
PTF 09cj	0.019	II	10.40±0.03	0.30±0.07	8.10±0.03	-2.00±0.07	7.32±0.03
PTF 09ct	0.150	II	9.95±0.14	0.17±0.26	8.46±0.14	-1.33±0.26	2.76±0.38
PTF 09cu	0.057	II	10.47±0.04	0.68±0.08	8.19±0.04	-1.60±0.08	6.63±0.06
PTF 09dfk	0.016	Ib	8.96±0.31	-0.82±0.34	8.49±0.31	-1.29±0.34	0.76±0.02
PTF 09djl	0.184	II	10.09±0.15	-0.04±0.36	9.47±0.15	-0.65±0.36	1.03±0.21
PTF 09dra	0.077	II	10.57±0.07	0.81±0.08	7.80±0.07	-1.96±0.08	15.03±0.22
PTF 09due	0.029	II	10.25±0.03	0.70±0.07	7.93±0.03	-1.62±0.07	7.30±0.03
PTF 09dzt	0.087	Ic	9.98±0.06	0.44±0.16	7.18±0.06	-2.37±0.16	12.35±0.46
PTF 09ebq	0.024	II	9.75±0.04	0.02±0.08	8.51±0.04	-1.22±0.08	2.04±0.02
PTF 09fbf	0.021	II	10.05±0.03	0.60±0.07	7.97±0.03	-1.48±0.07	8.30±0.04
PTF 09fmk	0.063	II	5.24±0.14
PTF 09foy	0.060	II	10.20±0.09	0.52±0.13	7.67±0.09	-2.01±0.13	7.46±0.09
PTF 09g	0.040	II	9.55±0.04	0.18±0.08	7.84±0.04	-1.53±0.08	2.98±0.02
PTF 09gof	0.103	II	10.06±0.06	0.60±0.20	7.56±0.06	-1.91±0.20	8.63±0.24
PTF 09hdo	0.047	II	10.75±0.03	0.70±0.07	8.61±0.03	-1.44±0.07	5.63±0.03
PTF 09hgz	0.028	II	10.55±0.03	-0.40±0.07	8.38±0.03	-2.57±0.07	9.06±0.05
PTF 09iex	0.020	II	8.36±0.47	-1.10±0.50	6.98±0.47	-2.48±0.50	2.42±0.14
PTF 09ige	0.064	II	9.76±0.07	0.32±0.20	7.61±0.07	-1.83±0.20	5.51±0.08
PTF 09igz	0.086	II	9.40±0.08	-0.16±0.15	7.72±0.08	-1.84±0.15	2.89±0.17
PTF 09ism	0.029	II	9.56±0.19	-0.16±0.19	7.83±0.19	-1.89±0.19	3.34±0.07
PTF 09ps	0.106	Ic	9.29±0.08	-0.18±0.15	8.20±0.08	-1.27±0.15	2.80±0.14
PTF 09q	0.090	Ic	10.83±0.09	0.86±0.12	8.23±0.09	-1.74±0.12	8.95±0.11
PTF 09r	0.027	II	9.01±0.23	-1.16±0.46	8.45±0.23	-1.72±0.46	1.49±0.02
PTF 09sh	0.038	II	9.95±0.03	0.40±0.07	7.97±0.03	-1.58±0.07	4.76±0.08
PTF 09sk	0.035	Ic-BL	8.85±0.14	-0.38±0.23	7.79±0.14	-1.45±0.23	2.36±0.05
PTF 09t	0.039	II	9.60±0.03	0.34±0.10	7.69±0.03	-1.57±0.10	5.14±0.04
PTF 09tm	0.035	II	10.35±0.03	0.30±0.07	8.62±0.03	-1.43±0.07	4.80±0.02
PTF 09uj	0.065	II	9.78±0.08	0.20±0.19	7.69±0.08	-1.89±0.19	5.75±0.10
PTF 10aavz	0.062	Ic-BL	9.09±0.11	-0.55±0.17	8.00±0.11	-1.64±0.17	2.33±0.13
PTF 10bau	0.026	II	10.35±0.03	0.40±0.07	8.32±0.03	-1.63±0.07	4.62±0.02
PTF 10bhu	0.036	Ic	9.44±0.14	-0.05±0.17	7.78±0.14	-1.71±0.17	3.63±0.04
PTF 10bip	0.051	Ic	9.10±0.10	-0.43±0.21	8.10±0.10	-1.43±0.21	2.01±0.06
PTF 10con	0.033	II	0.37±62.69
PTF 10cqh	0.041	II	10.77±0.04	0.97±0.08	8.51±0.04	-1.29±0.08	6.80±0.04
PTF 10cwv	0.073	II	9.65±0.08	0.08±0.18	7.80±0.08	-1.78±0.18	3.68±0.30
PTF 10cxq	0.047	II	8.93±0.11	-0.13±0.23	7.38±0.11	-1.68±0.23	5.86±0.14

Name	z	Type	Mass ($\log M_{\odot}$)	SFR (phot) ($\log M_{\odot} \text{ yr}^{-1}$)	Σ_M ($\log M_{\odot} \text{ kpc}^{-2}$)	Σ_{SFR} ($\log M_{\odot} \text{ yr}^{-1} \text{ kpc}^{-2}$)	r_{50} (kpc)
PTF 10cxx	0.034	II	10.27±0.13	0.24±0.17	8.88±0.13	-1.15±0.17	2.62±0.02
PTF 10czn	0.045	II	10.45±0.04	0.96±0.09	7.74±0.04	-1.75±0.09	9.71±0.05
PTF 10dk	0.074	II	8.54±0.19	-1.06±0.18	7.64±0.19	-1.96±0.18	1.47±0.51
PTF 10hv	0.052	II	11.22±0.04	1.60±0.07	9.17±0.04	-0.46±0.07	6.85±0.11
PTF 10qts	0.091	Ic-BL	9.60±0.09	-0.91±0.30	8.83±0.09	-1.68±0.30	1.17±0.36
PTF 10s	0.051	II	9.62±0.09	-0.09±0.15	7.98±0.09	-1.73±0.15	2.97±0.06
PTF 11cgx	0.033	II	9.92±0.13	0.41±0.17	8.19±0.13	-1.32±0.17	3.48±0.02
PTF 11cwi	0.056	II	10.56±0.04	0.51±0.08	8.54±0.04	-1.51±0.08	4.63±0.08
PTF 11dad	0.072	II	9.97±0.08	0.33±0.15	7.93±0.08	-1.71±0.15	7.48±0.15
PTF 11dqk	0.036	II	9.85±0.03	0.45±0.13	7.95±0.03	-1.45±0.13	3.93±0.02
PTF 11dqr	0.082	II	9.34±0.10	-0.21±0.19	6.64±0.10	-2.91±0.19	10.25±0.98
PTF 11dsb	0.190	II	9.70±0.08	0.23±0.16	7.28±0.08	-2.18±0.16	7.42±0.57
PTF 11dtd	0.040	II	10.25±0.03	0.80±0.07	7.75±0.03	-1.70±0.07	9.01±0.06
PTF 11ecp	0.034	II	10.00±0.03	0.60±0.07	8.05±0.03	-1.35±0.07	6.36±0.04
PTF 11ekj	0.043	II	9.92±0.12	-0.35±0.15	10.10±0.12	-0.18±0.15	0.43±0.08
PTF 11emc	0.082	II	9.22±0.09	-0.38±0.18	7.68±0.09	-1.92±0.18	3.97±0.23
PTF 11epi	0.032	II	11.00±0.03	0.10±0.07	8.48±0.03	-2.42±0.07	11.21±0.06
PTF 11ftr	0.018	II	7.80±0.32	-0.84±0.36	7.31±0.32	-1.33±0.36	0.84±0.01
PTF 11fuu	0.097	II	10.34±0.05	0.47±0.09	8.56±0.05	-1.30±0.09	4.02±0.08
PTF 11fuv	0.030	II	11.15±0.03	1.20±0.07	8.76±0.03	-1.19±0.07	7.24±0.04
PTF 11gdz	0.013	II	10.39±0.04	0.38±0.08	9.40±0.04	-0.61±0.08	1.29±0.01
PTF 11hyg	0.030	Ic	10.84±0.04	1.02±0.07	8.32±0.04	-1.50±0.07	7.81±0.03
PTF 11iqb	0.013	II	11.59±0.32	1.58±0.35	9.34±0.32	-0.68±0.35	5.93±0.03
PTF 11ixk	0.021	Ic	10.26±0.04	0.60±0.07	8.19±0.04	-1.46±0.07	5.48±0.02
PTF 11izq	0.062	Ib	9.23±0.09	-0.33±0.17	7.24±0.09	-2.31±0.17	4.66±0.18
PTF 11jgp	0.070	II	9.91±0.04	0.54±0.10	7.95±0.04	-1.42±0.10	4.78±0.07
PTF 11kjk	0.067	II	9.12±0.10	-0.17±0.20	7.44±0.10	-1.85±0.20	5.67±0.25
PTF 11klg	0.027	Ic	10.62±0.19	0.44±0.22	8.56±0.19	-1.62±0.22	5.15±0.04
PTF 11kqn	0.066	II	11.26±0.05	1.09±0.07	8.89±0.05	-1.29±0.07	8.06±0.08
PTF 11ktr	0.106	II	10.45±0.04	0.80±0.07	8.03±0.04	-1.63±0.07	8.32±0.18
PTF 11mhh	0.039	II	9.96±0.15	0.22±0.15	7.95±0.15	-1.79±0.15	4.45±0.07
PTF 11mmk	0.049	II	9.55±0.11	-0.16±0.14	8.10±0.11	-1.60±0.14	3.75±0.07
PTF 11mpv	0.043	II	9.26±0.09	-0.14±0.12	8.18±0.09	-1.22±0.12	2.58±0.04
PTF 11pdj	0.024	II	10.85±0.03	-0.20±0.07	8.96±0.03	-2.09±0.07	9.74±0.07
PTF 11qcc	0.043	II	9.73±0.12	-0.11±0.15	8.19±0.12	-1.65±0.15	6.11±0.12
PTF 11qcm	0.050	II	10.60±0.19	0.61±0.19	8.43±0.19	-1.57±0.19	7.71±0.05
PTF 11qgw	0.027	II	8.98±0.19	-0.27±0.29	7.16±0.19	-2.09±0.29	6.88±0.10
PTF 11qju	0.028	II	9.12±0.18	-0.41±0.23	10.24±0.18	0.71±0.23	0.15±0.34
PTF 11qux	0.041	II	0.66±0.01
PTF 12boj	0.037	II	10.58±0.16	0.57±0.17	8.53±0.16	-1.48±0.17	4.47±0.02
PTF 12bpy	0.060	II	9.36±0.14	-0.15±0.22	8.70±0.14	-0.80±0.22	0.96±0.04
PTF 12bwq	0.040	Ib	9.53±0.22	-0.11±0.27	7.07±0.22	-2.57±0.27	9.62±0.21
PTF 12cdc	0.070	II	10.78±0.11	0.77±0.14	7.77±0.11	-2.25±0.14	15.31±0.16
PTF 12cde	0.013	Ib/c	8.36±0.32	-1.17±0.38	7.03±0.32	-2.50±0.38	3.61±0.12
PTF 12cgb	0.026	II	9.27±0.04	-0.14±0.12	7.99±0.04	-1.42±0.12	2.61±0.01
PTF 12dke	0.067	II	9.91±0.08	0.46±0.15	7.40±0.08	-2.05±0.15	11.27±0.20
PTF 12eje	0.078	II	9.92±0.07	0.49±0.18	7.82±0.07	-1.61±0.18	5.60±0.07
PTF 12fes	0.036	Ib	10.55±0.04	0.99±0.07	7.98±0.04	-1.58±0.07	8.51±0.07
PTF 12gex	0.045	II	9.74±0.04	0.48±0.08	7.42±0.04	-1.84±0.08	7.16±0.09
PTF 12gyr	0.056	Ib/c	10.60±0.03	1.08±0.08	8.07±0.03	-1.46±0.08	9.24±0.04
PTF 12gzk	0.014	12gzk	7.47±0.11	-1.46±0.38	7.43±0.11	-1.50±0.38	0.54±0.05
PTF 12ije	0.042	II	10.01±0.12	0.27±0.16	7.89±0.12	-1.84±0.16	5.37±0.08
PTF 12ne	0.033	II	9.91±0.13	-0.06±0.17	8.62±0.13	-1.35±0.17	1.82±0.02
PTF 13bvn	0.004	Ib	11.10±0.03	1.00±0.07	9.66±0.03	-0.44±0.07	2.68±0.02
PTF 13c	0.011	II	9.04±0.04	-0.70±0.07	8.00±0.04	-1.74±0.07	1.56±0.01

Name	z	Type	Mass ($\log M_{\odot}$)	SFR (phot) ($\log M_{\odot} \text{ yr}^{-1}$)	Σ_M ($\log M_{\odot} \text{ kpc}^{-2}$)	Σ_{SFR} ($\log M_{\odot} \text{ yr}^{-1} \text{ kpc}^{-2}$)	r_{50} (kpc)
PTF 13cab	0.030	Ib	9.32±0.30	-0.28±0.37	7.72±0.30	-1.88±0.37	4.39±0.06
PTF 13cac	0.030	II	8.91±0.31	-0.87±0.37	7.38±0.31	-2.40±0.37	3.97±0.13
PTF 13cbf	0.039	Ic	9.40±0.03	-0.00±0.07	7.72±0.03	-1.68±0.07	5.78±0.06
PTF 13d	0.024	II	10.25±0.04	0.60±0.07	8.07±0.04	-1.58±0.07	6.27±0.02
SN 1999ap	0.040	II	9.35±0.12	-0.04±0.18	7.33±0.12	-2.06±0.18	5.25±0.10
SN 1999as	0.127	Ic pec	9.02±1.05
SN 1999bc	0.021	Ic	10.46±0.04	0.62±0.08	8.18±0.04	-1.66±0.08	6.74±0.03
SN 1999bd	0.151	II	9.66±0.09	0.07±0.16	8.58±0.09	-1.01±0.16	2.86±0.28
SN 2001bk	0.043	II	8.82±0.13	-0.79±0.19	7.58±0.13	-2.02±0.19	3.13±0.15
SN 2001fb	0.032	II	9.95±0.03	0.60±0.07	8.53±0.03	-0.82±0.07	3.46±0.02
SN 2001ij	0.038	II P	10.20±0.03	0.40±0.07	8.22±0.03	-1.59±0.07	5.55±0.04
SN 2002dg	0.047	Ib	9.10±0.11	0.06±0.16	7.10±0.11	-1.94±0.16	4.31±0.07
SN 2002ew	0.030	II	9.36±0.04	-0.08±0.11	7.95±0.04	-1.49±0.11	2.76±0.02
SN 2002fa	0.060	II	10.12±0.09	0.59±0.20	7.43±0.09	-2.10±0.20	9.16±0.11
SN 2002fu	0.091	II	9.86±0.07	0.25±0.14	7.90±0.07	-1.72±0.14	9.06±0.21
SN 2002hj	0.024	II	9.60±0.20	-0.02±0.26	7.75±0.20	-1.87±0.26	4.04±0.05
SN 2002ik	0.032	II P	10.55±0.03	0.70±0.07	8.52±0.03	-1.33±0.07	5.92±0.03
SN 2002in	0.076	II	9.11±0.09	-0.48±0.19	7.64±0.09	-1.96±0.19	4.15±0.33
SN 2002ip	0.079	II	8.90±0.10	-0.61±0.19	6.76±0.10	-2.75±0.19	5.55±0.80
SN 2002iq	0.056	II	9.38±0.06	0.13±0.14	7.81±0.06	-1.44±0.14	3.98±0.18
SN 2002jl	0.064	II	8.01±0.23	-1.23±0.22	7.30±0.23	-1.93±0.22	1.37±0.33
SN 2003cv	0.028	II pec	8.31±0.20	-0.96±0.27	7.40±0.20	-1.86±0.27	1.90±0.05
SN 2003dq	0.046	II	9.01±0.12	-0.43±0.16	7.59±0.12	-1.85±0.16	2.95±0.12
SN 2003kj	0.100	II	8.77±0.18	-0.79±0.18	7.14±0.18	-2.43±0.18	3.04±0.78
SN 2004cm	0.004	II P	9.65±0.03	0.00±0.07	8.51±0.03	-1.14±0.07	1.75±0.01
SN 2004gy	0.027	II	8.26±0.20	-1.02±0.26	7.44±0.20	-1.83±0.26	1.63±0.05
SN 2004ht	0.067	II	10.30±0.07	0.60±0.09	7.97±0.07	-1.72±0.09	7.58±0.09
SN 2004hv	0.061	II	8.82±0.13	-0.70±0.19	6.90±0.13	-2.62±0.19	5.27±0.98
SN 2004hx	0.014	II	8.69±0.31	-1.11±0.35	7.72±0.31	-2.08±0.35	1.63±0.02
SN 2004ic	0.093	II	10.92±0.06	1.03±0.08	7.80±0.06	-2.09±0.08	15.04±0.30
SN 2005bn	0.028	II	9.14±0.20	-0.44±0.28	8.30±0.20	-1.28±0.28	1.38±0.01
SN 2005fq	0.140	II	8.83±0.14	-0.54±0.18	7.46±0.14	-1.91±0.18	3.35±1.08
SN 2005gi	0.050	II	9.12±0.14	-0.39±0.16	7.10±0.14	-2.41±0.16	4.74±0.26
SN 2005hl	0.020	Ib	10.40±0.04	0.40±0.07	8.91±0.04	-1.09±0.07	2.94±0.01
SN 2005hm	0.030	Ib	8.61±0.30	-1.53±0.34	8.28±0.30	-1.87±0.34	0.94±0.19
SN 2005kb	0.015	II	9.35±0.31	-0.43±0.39	8.19±0.31	-1.59±0.39	4.32±0.05
SN 2005kr	0.130	Ic-BL	8.63±0.16	-0.62±0.20	8.36±0.16	-0.88±0.20	0.57±0.30
SN 2005ks	0.100	Ic-BL	9.88±0.08	0.27±0.14	8.44±0.08	-1.17±0.14	3.70±0.08
SN 2005lb	0.030	II	8.75±0.30	-0.94±0.32	7.47±0.30	-2.22±0.32	3.95±0.37
SN 2005lc	0.010	II	8.21±0.33	-1.34±0.39	7.41±0.33	-2.13±0.39	1.32±0.06
SN 2005lm	0.080	II	9.23±0.08	-0.24±0.16	8.01±0.08	-1.46±0.16	1.83±0.07
SN 2005mk	0.150	II	9.44±0.09	-0.16±0.17	7.50±0.09	-2.09±0.17	4.13±0.64
SN 2005mn	0.050	Ib	9.61±0.16	0.17±0.22	7.46±0.16	-1.97±0.22	11.24±0.26
SN 2006L	0.039	II n	8.28±0.16	-1.19±0.19	7.63±0.16	-1.84±0.19	1.18±0.08
SN 2006M	0.015	II n	9.05±0.03	-0.42±0.08	7.73±0.03	-1.74±0.08	1.93±0.01
SN 2006ad	0.030	II	8.97±0.05	-1.27±0.10	11.66±0.05	1.42±0.10	0.02±0.02
SN 2006ag	0.035	II n	8.05±0.16	-0.63±0.18	6.91±0.16	-1.77±0.18	1.74±0.08
SN 2006aj	0.033	Ic-BL	8.08±0.17	-1.31±0.25	8.01±0.17	-1.38±0.25	0.46±0.10
SN 2006bj	0.038	II	9.38±0.15	-0.08±0.19	7.32±0.15	-2.15±0.19	4.80±0.07
SN 2006cu	0.029	II n	10.15±0.03	0.50±0.07	7.79±0.03	-1.86±0.07	7.15±0.02
SN 2006cv	0.100	II n	10.33±0.05	-0.60±0.07	8.61±0.05	-2.32±0.07	3.18±0.22
SN 2006cw	0.065	II	10.02±0.06	0.50±0.09	7.82±0.06	-1.70±0.09	6.72±0.11
SN 2006cy	0.036	II n	10.21±0.04	0.69±0.08	7.88±0.04	-1.63±0.08	6.07±0.03
SN 2006db	0.023	II n	8.69±0.19	-0.59±0.24	7.40±0.19	-1.88±0.24	2.39±0.04
SN 2006fg	0.030	II	7.99±0.30	-1.53±0.32	8.17±0.30	-1.35±0.32	0.34±0.03

Name	z	Type	Mass ($\log M_{\odot}$)	SFR (phot) ($\log M_{\odot} \text{ yr}^{-1}$)	Σ_M ($\log M_{\odot} \text{ kpc}^{-2}$)	Σ_{SFR} ($\log M_{\odot} \text{ yr}^{-1} \text{ kpc}^{-2}$)	r_{50} (kpc)
SN 2006fo	0.021	Ib	10.25±0.03	0.50±0.07	8.53±0.03	-1.22±0.07	3.18±0.01
SN 2006fq	0.070	II P	9.96±0.04	0.50±0.07	8.13±0.04	-1.34±0.07	4.61±0.04
SN 2006gd	0.150	II P	10.97±0.07	0.86±0.16	8.23±0.07	-1.89±0.16	15.45±0.42
SN 2006gy	0.019	II n	11.17±0.32	0.54±0.35	9.36±0.32	-1.27±0.35	4.74±0.03
SN 2006ho	0.110	II	11.25±0.03	0.80±0.07	9.01±0.03	-1.44±0.07	6.09±0.09
SN 2006ic	0.040	II	10.45±0.04	0.70±0.07	8.17±0.04	-1.58±0.07	5.95±0.04
SN 2006ih	0.130	II	8.95±0.18	-0.30±0.20	9.55±0.18	0.30±0.20	0.24±0.09
SN 2006ii	0.030	II	9.44±0.30	-0.32±0.31	7.51±0.30	-2.25±0.31	4.11±0.07
SN 2006ij	0.040	II	9.81±0.11	0.28±0.16	7.74±0.11	-1.79±0.16	6.70±0.06
SN 2006ip	0.030	Ic	9.64±0.19	0.15±0.19	7.87±0.19	-1.61±0.19	3.61±0.03
SN 2006ir	0.020	Ic	8.77±0.32	-0.85±0.35	7.11±0.32	-2.51±0.35	3.49±0.05
SN 2006iw	0.030	II	9.67±0.29	-0.02±0.31	8.06±0.29	-1.63±0.31	4.19±0.09
SN 2006ix	0.080	II	9.65±0.11	-0.02±0.19	7.79±0.11	-1.88±0.19	7.91±0.23
SN 2006kh	0.060	II	9.46±0.08	-0.23±0.13	8.97±0.08	-0.72±0.13	0.81±0.02
SN 2006kn	0.120	II	9.51±0.07	0.10±0.19	7.30±0.07	-2.12±0.19	10.94±0.58
SN 2006lc	0.016	Ib	10.65±0.03	0.40±0.07	8.59±0.03	-1.66±0.07	5.27±0.02
SN 2006lh	0.032	II	7.95±0.18	-1.41±0.22	7.71±0.18	-1.65±0.22	0.62±0.06
SN 2006ls	0.140	I pec	9.88±0.08	0.25±0.16	7.33±0.08	-2.30±0.16	11.10±0.56
SN 2006lt	0.015	Ib	8.82±0.34	-1.01±0.35	9.60±0.34	-0.23±0.35	0.18±0.08
SN 2006nq	0.025	II	9.38±0.19	-0.11±0.19	7.40±0.19	-2.09±0.19	4.86±0.05
SN 2006ns	0.120	II	9.81±0.04	0.54±0.15	7.77±0.04	-1.50±0.15	6.99±0.14
SN 2006nx	0.050	Ic-BL	8.57±0.17	-0.98±0.25	7.40±0.17	-2.16±0.25	1.79±0.20
SN 2006ny	0.080	II P	10.22±0.05	0.18±0.09	8.41±0.05	-1.63±0.09	7.10±0.15
SN 2006qk	0.060	Ic-BL	9.61±0.13	-0.31±0.17	8.89±0.13	-1.03±0.17	1.71±0.05
SN 2006rc	0.080	II n	9.88±0.11	0.25±0.17	7.70±0.11	-1.93±0.17	6.60±0.15
SN 2006rq	0.070	II	10.86±0.04	0.02±0.07	8.67±0.04	-2.17±0.07	8.67±0.08
SN 2006ru	0.020	II	11.15±0.03	0.10±0.07	10.25±0.03	-0.80±0.07	1.63±0.00
SN 2006ry	0.060	II	10.95±0.03	...	9.51±0.03	...	4.05±0.07
SN 2006tf	0.074	II n	8.16±0.17	-0.97±0.21	8.84±0.17	-0.29±0.21	0.61±1.85
SN 2006th	0.140	II	4.24±0.97
SN 2007I	0.022	Ic-BL	8.92±0.21	-0.75±0.26	7.78±0.21	-1.88±0.26	1.92±0.05
SN 2007bg	0.034	Ic-BL	7.99±0.23	-2.03±0.33	8.21±0.23	-1.81±0.33	0.39±0.16
SN 2007bo	0.040	II	9.13±0.21	-0.33±0.28	7.35±0.21	-2.10±0.28	3.61±0.08
SN 2007bp	0.030	II	10.80±0.14	1.00±0.22	7.99±0.14	-1.81±0.22	10.71±0.06
SN 2007bt	0.040	II n	9.65±0.22	-0.03±0.29	7.62±0.22	-2.07±0.29	4.85±0.06
SN 2007bu	0.030	II	8.46±0.30	-1.26±0.34	7.67±0.30	-2.05±0.34	1.54±0.10
SN 2007bv	0.050	II	11.34±0.09	1.10±0.15	8.65±0.09	-1.59±0.15	11.25±0.09
SN 2007bw	0.140	II n	9.66±0.08	0.40±0.15	7.45±0.08	-1.81±0.15	5.43±0.28
SN 2007bx	0.020	II	8.16±0.48	-1.24±0.51	7.19±0.48	-2.21±0.51	2.16±0.14
SN 2007by	0.040	II	10.23±0.13	0.42±0.19	8.00±0.13	-1.81±0.19	6.11±0.04
SN 2007ce	0.046	Ic-BL	8.08±0.13	-0.60±0.16	8.03±0.13	-0.66±0.16	0.45±0.19
SN 2007dp	0.030	II	9.14±0.28	-0.52±0.33	8.03±0.28	-1.63±0.33	1.77±0.02
SN 2007dq	0.050	II	8.71±0.20	-1.01±0.28	7.14±0.20	-2.58±0.28	3.42±0.39
SN 2007dw	0.050	II	10.07±0.06	0.59±0.09	7.80±0.06	-1.69±0.09	6.10±0.04
SN 2007dy	0.040	Ib	9.21±0.22	-0.32±0.27	7.29±0.22	-2.24±0.27	3.71±0.12
SN 2007eb	0.040	Ic-BL	8.50±0.22	-0.78±0.30	7.22±0.22	-2.06±0.30	3.31±0.16
SN 2007ed	0.070	II	10.69±0.11	0.54±0.15	8.71±0.11	-1.44±0.15	4.87±0.08
SN 2007eh	0.010	II	8.04±0.32	-1.32±0.39	9.05±0.32	-0.32±0.39	0.15±0.06
SN 2007ei	0.030	II	9.53±0.30	-0.13±0.34	7.21±0.30	-2.45±0.34	6.23±0.17
SN 2007em	0.030	II	7.63±0.31	-1.54±0.36	7.00±0.31	-2.17±0.36	1.21±0.25
SN 2007eq	0.030	Ib/c	8.49±0.30	-1.14±0.32	7.47±0.30	-2.17±0.32	2.80±0.16
SN 2007er	0.070	II	9.62±0.12	0.08±0.16	7.32±0.12	-2.22±0.16	6.69±0.19
SN 2007es	0.030	II	10.94±0.04	0.99±0.08	8.56±0.04	-1.39±0.08	7.46±0.08
SN 2007et	0.040	II	10.00±0.04	0.41±0.08	7.71±0.04	-1.89±0.08	6.38±0.03
SN 2007eu	0.040	II	9.33±0.05	-0.03±0.13	7.40±0.05	-1.96±0.13	3.92±0.06

Name	z	Type	Mass ($\log M_{\odot}$)	SFR (phot) ($\log M_{\odot} \text{ yr}^{-1}$)	Σ_M ($\log M_{\odot} \text{ kpc}^{-2}$)	Σ_{SFR} ($\log M_{\odot} \text{ yr}^{-1} \text{ kpc}^{-2}$)	r_{50} (kpc)
SN 2007ew	0.030	II	9.38±0.30	-0.40±0.36	7.54±0.30	-2.24±0.36	4.78±0.14
SN 2007fa	0.060	II	11.07±0.09	1.05±0.10	8.54±0.09	-1.48±0.10	8.70±0.10
SN 2007fe	0.030	II	9.39±0.21	-0.38±0.23	7.89±0.21	-1.88±0.23	2.63±0.02
SN 2007ff	0.050	Ic	10.45±0.13	0.64±0.18	8.09±0.13	-1.72±0.18	6.45±0.06
SN 2007fg	0.030	II	8.87±0.20	-0.35±0.29	7.12±0.20	-2.10±0.29	3.81±0.08
SN 2007fk	0.040	IIn	8.61±0.22	-1.05±0.41	7.04±0.22	-2.62±0.41	3.64±0.20
SN 2007fw	0.050	IIn	9.05±0.18	-0.52±0.22	7.74±0.18	-1.83±0.22	3.91±0.15
SN 2007fy	0.050	II	9.96±0.04	0.61±0.07	8.00±0.04	-1.35±0.07	5.62±0.04
SN 2007fz	0.014	II	8.44±0.31	-1.22±0.32	7.85±0.31	-1.81±0.32	1.54±0.01
SN 2007gh	0.020	II	9.45±0.30	-0.30±0.33	8.70±0.30	-1.05±0.33	1.10±0.01
SN 2007gl	0.030	Ic	9.90±0.17	0.20±0.17	7.39±0.17	-2.31±0.17	7.37±0.07
SN 2007gm	0.030	II	9.13±0.31	-0.51±0.43	8.05±0.31	-1.59±0.43	1.48±0.03
SN 2007gs	0.040	II	9.57±0.13	-0.01±0.12	7.40±0.13	-2.18±0.12	6.47±0.12
SN 2007gy	0.040	IIn	9.34±0.22	-0.22±0.23	7.26±0.22	-2.29±0.23	4.40±0.18
SN 2007gz	0.050	II	9.80±0.18	0.01±0.19	9.01±0.18	-0.78±0.19	1.01±0.01
SN 2007hb	0.022	Ic	10.55±0.03	0.80±0.07	8.51±0.03	-1.24±0.07	4.87±0.01
SN 2007hi	0.070	II	8.11±0.35	-1.49±0.26	10.20±0.35	0.59±0.26	0.06±0.12
SN 2007hn	0.030	Ic	9.86±0.30	-0.03±0.30	8.29±0.30	-1.60±0.30	3.30±0.04
SN 2007hs	0.070	II	8.68±0.20	-1.11±0.28	7.65±0.20	-2.15±0.28	2.50±0.75
SN 2007hw	0.080	II	10.85±0.03	1.00±0.07	8.55±0.03	-1.30±0.07	7.15±0.06
SN 2007ib	0.030	II	9.52±0.18	-0.02±0.30	7.69±0.18	-1.86±0.30	4.31±0.03
SN 2007iu	0.090	II	9.31±0.13	-0.35±0.15	6.59±0.13	-3.07±0.15	9.77±0.24
SN 2007ja	0.090	II P	10.65±0.03	1.00±0.07	8.22±0.03	-1.43±0.07	7.78±0.08
SN 2007jf	0.070	II P	9.65±0.13	-0.03±0.21	7.78±0.13	-1.90±0.21	5.06±0.19
SN 2007jm	0.090	II n	9.77±0.10	0.10±0.16	8.34±0.10	-1.34±0.16	4.36±0.19
SN 2007jn	0.060	II	8.99±0.14	-0.38±0.21	7.54±0.14	-1.84±0.21	4.79±0.24
SN 2007kw	0.070	II	10.82±0.06	0.72±0.08	8.67±0.06	-1.44±0.08	6.24±0.07
SN 2007ky	0.070	II	10.85±0.03	0.90±0.07	8.02±0.03	-1.93±0.07	14.62±0.12
SN 2007kz	0.130	II	11.20±0.05	1.36±0.09	8.14±0.05	-1.70±0.09	16.25±0.21
SN 2007lb	0.060	II	1.90±0.67
SN 2007ld	0.030	II	7.96±0.30	-1.35±0.34	6.54±0.30	-2.77±0.34	2.72±0.43
SN 2007lj	0.040	II	8.06±0.24	-1.27±0.28	8.43±0.24	-0.90±0.28	0.51±0.90
SN 2007lz	0.090	II	9.30±0.12	-0.39±0.20	7.18±0.12	-2.51±0.20	5.65±0.49
SN 2007md	0.050	II	10.93±0.10	0.97±0.14	8.57±0.10	-1.40±0.14	9.00±0.04
SN 2007ms	0.040	II pec	8.50±0.22	-0.57±0.27	7.70±0.22	-1.37±0.27	1.70±0.09
SN 2007nm	0.046	Ic	8.47±0.22	-1.72±0.35	8.87±0.22	-1.32±0.35	0.36±0.22
SN 2007nr	0.140	II P	9.46±0.07	0.00±0.18	7.67±0.07	-1.79±0.18	3.54±0.26
SN 2007nw	0.060	II P	10.26±0.05	0.42±0.08	8.19±0.05	-1.65±0.08	5.68±0.09
SN 2007ny	0.140	II P	9.11±0.18	-0.66±0.24	7.52±0.18	-2.25±0.24	6.39±3.82
SN 2007qb	0.080	II	10.27±0.07	0.73±0.15	7.53±0.07	-2.01±0.15	10.93±0.18
SN 2007qv	0.100	II	10.51±0.10	0.57±0.12	8.32±0.10	-1.63±0.12	6.88±0.17
SN 2007qw	0.150	Ic-BL	9.40±0.05	0.13±0.13	8.31±0.05	-0.96±0.13	1.84±0.22
SN 2007qx	0.060	Ib	10.03±0.11	0.34±0.15	7.90±0.11	-1.80±0.15	6.87±0.08
SN 2007sd	0.090	II P	8.95±0.11	-0.48±0.19	7.38±0.11	-2.06±0.19	4.73±0.61
SN 2007sj	0.040	Ib/c	10.45±0.03	0.80±0.07	8.01±0.03	-1.64±0.07	7.09±0.03
SN 2007sx	0.120	II	10.96±0.04	1.05±0.10	7.84±0.04	-2.07±0.10	16.58±0.29
SN 2007sz	0.020	II	8.56±0.31	-0.98±0.31	7.21±0.31	-2.34±0.31	2.20±0.04
SN 2007tn	0.050	II	10.27±0.16	0.36±0.16	8.18±0.16	-1.73±0.16	4.56±0.06
SN 2008bj	0.019	II	8.54±0.28	-0.95±0.28	6.92±0.28	-2.57±0.28	3.24±0.04
SN 2008fm	0.039	IIn	11.29±0.13	1.28±0.14	8.30±0.13	-1.71±0.14	17.13±0.10
SN 2008fn	0.030	Ib/c	9.86±0.20	-0.56±0.30	8.33±0.20	-2.09±0.30	2.63±0.03
SN 2008fo	0.030	Ic	9.50±0.04	-0.07±0.09	7.70±0.04	-1.87±0.09	4.20±0.02
SN 2008fs	0.039	Ib/c	10.19±0.05	0.25±0.11	8.29±0.05	-1.65±0.11	4.15±0.04
SN 2008fz	0.133	IIn	9.93±0.05	1.25±0.10	13.12±0.05	4.44±0.10	0.01±0.08
SN 2008gd	0.059	II	9.89±0.09	0.47±0.14	7.42±0.09	-2.00±0.14	7.67±0.10

Name	z	Type	Mass ($\log M_{\odot}$)	SFR (phot) ($\log M_{\odot} \text{ yr}^{-1}$)	Σ_M ($\log M_{\odot} \text{ kpc}^{-2}$)	Σ_{SFR} ($\log M_{\odot} \text{ yr}^{-1} \text{ kpc}^{-2}$)	r_{50} (kpc)
SN 2008iu	0.130	Ic-BL	8.22±0.28	-0.72±0.23	8.26±0.28	-0.68±0.23	0.63±1.21
SN 2008iy	0.041	IIn	10.20±0.03	-0.10±0.07	18.89±0.03	8.59±0.07	0.00±0.00
SN 2008ja	0.069	IIn	8.38±0.20	-1.21±0.21	7.85±0.20	-1.74±0.21	1.35±0.37
SN 2009W	0.017	II P	8.92±0.32	-0.69±0.34	7.23±0.32	-2.39±0.34	3.06±0.12
SN 2009bh	0.090	Ic	10.83±0.10	0.86±0.12	8.23±0.10	-1.74±0.12	8.95±0.11
SN 2009bj	0.027	II	9.01±0.23	-1.16±0.46	8.45±0.23	-1.72±0.46	1.49±0.02
SN 2009bk	0.039	II	9.60±0.03	0.33±0.09	7.69±0.03	-1.58±0.09	5.14±0.04
SN 2009bl	0.040	II	9.55±0.04	0.18±0.08	7.84±0.04	-1.53±0.08	2.98±0.02
SN 2009ct	0.060	II	10.47±0.06	0.69±0.09	8.15±0.06	-1.64±0.09	6.98±0.06
SN 2009dh	0.060	II P	7.99±0.19	-1.54±0.25	7.80±0.19	-1.73±0.25	0.61±0.33
SN 2009di	0.130	Ic	8.57±0.24	-0.47±0.22	6.98±0.24	-2.07±0.22	3.54±1.26
SN 2009dw	0.042	II P	7.97±0.27	-1.45±0.23	6.35±0.27	-3.07±0.23	3.51±1.06
SN 2009fe	0.047	II	10.80±0.03	-0.09±0.08	9.59±0.03	-1.30±0.08	1.82±0.02
SN 2009jd	0.025	II	9.40±0.19	-0.08±0.20	7.16±0.19	-2.31±0.20	5.67±0.07
SN 2009kf	0.182	II P	9.66±0.09	0.14±0.19	7.98±0.09	-1.54±0.19	4.10±0.55
SN 2009lx	0.027	II P	10.45±0.03	0.51±0.07	8.37±0.03	-1.57±0.07	4.79±0.03
SN 2009nn	0.046	IIn	9.76±0.05	0.21±0.08	7.79±0.05	-1.76±0.08	5.20±0.06
SN 2009nu	0.040	II	9.24±0.22	-0.56±0.29	7.02±0.22	-2.77±0.29	5.84±0.28
SN 2010K	0.020	II	8.36±0.47	-1.10±0.50	6.98±0.47	-2.48±0.50	2.42±0.14
SN 2010Q	0.055	Ic	7.46±0.20	-1.18±0.22	6.80±0.20	-1.83±0.22	1.03±0.40
SN 2010ah	0.050	Ic-BL	8.82±0.13	-0.85±0.20	7.67±0.13	-2.00±0.20	4.43±0.27
SN 2010ay	0.067	Ic-BL	8.58±0.09	0.03±0.11	8.92±0.09	0.37±0.11	0.34±0.02
SN 2010gq	0.018	II	10.50±0.03	0.50±0.07	8.63±0.03	-1.38±0.07	4.64±0.02
SN 2010jc	0.024	II P	10.75±0.03	0.70±0.07	7.92±0.03	-2.13±0.07	11.07±0.08
SN 2010jy	0.042	IIn	9.11±0.12	-0.50±0.18	7.58±0.12	-2.04±0.18	2.73±0.11
SN 2010mb	0.133	Ic	9.63±0.07	0.14±0.16	7.56±0.07	-1.93±0.16	8.76±0.32
SN 2011ak	0.027	II P	10.45±0.03	0.50±0.07	7.95±0.03	-2.00±0.07	7.73±0.05
SN 2011an	0.016	IIn	9.61±0.04	-0.02±0.07	7.23±0.04	-2.39±0.07	7.18±0.04
SN 2011aw	0.055	Ib/c	1.67±1.37
SN 2011bm	0.022	Ic	9.45±0.03	0.10±0.07	7.88±0.03	-1.47±0.07	2.67±0.01
SN 2011bn	0.031	II	11.20±0.03	1.20±0.07	8.80±0.03	-1.20±0.07	8.83±0.06
SN 2011bs	0.036	II	7.44±0.28	-2.12±0.26	8.43±0.28	-1.12±0.26	0.56±0.18
SN 2011cl	0.025	II P	8.76±0.07
SN 2011cq	0.017	II pec	9.69±0.31	0.13±0.34	7.41±0.31	-2.15±0.34	5.51±0.03
SN 2011cw	0.040	IIn	0.59±0.28
SN 2011cz	0.060	II P	8.24±0.22	-1.24±0.25	7.32±0.22	-2.16±0.25	3.03±2.16
SN 2011db	0.025	II	9.68±0.19	0.14±0.27	7.50±0.19	-2.04±0.27	5.19±0.03
SN 2011en	0.020	II P	8.70±0.46	-0.48±0.42	7.29±0.46	-1.89±0.42	2.46±0.05
SN 2011eo	0.030	II P	8.02±0.30	-1.57±0.33	7.80±0.30	-1.78±0.33	0.62±0.07
SN 2011eu	0.110	IIn	9.54±0.15	-0.38±0.34	9.76±0.15	-0.17±0.34	1.39±0.98
SN 2011ev	0.030	II P	8.99±0.27	-0.23±0.33	7.08±0.27	-2.14±0.33	7.65±0.11
SN 2011ew	0.070	II P	10.19±0.04	-0.80±0.07	9.92±0.04	-1.07±0.07	0.98±0.78
SN 2011fa	0.060	II P	7.85±0.23	-1.61±0.25	7.69±0.23	-1.76±0.25	0.57±0.25
SN 2011fz	0.016	Ib/c	10.55±0.03	0.60±0.07	8.00±0.03	-1.95±0.07	7.92±0.06
SN 2011hn	0.014	II P	10.02±0.31	0.15±0.33	8.20±0.31	-1.67±0.33	6.02±0.02
SN 2011iw	0.023	IIn	7.92±0.22	-1.64±0.23	7.97±0.22	-1.59±0.23	0.48±0.05
SN 2011jb	0.084	IIn	9.20±0.09	-0.46±0.18	8.48±0.09	-1.18±0.18	1.24±0.11
SN 2011jj	0.045	II P	10.99±0.04	1.10±0.07	8.05±0.04	-1.84±0.07	13.98±0.09
SN 2011ke	0.143	Ic	8.91±0.15	-0.42±0.19	6.86±0.15	-2.47±0.19	6.77±1.61
SN 2012D	0.026	II P	9.60±0.04	0.01±0.07	8.12±0.04	-1.48±0.07	2.57±0.01
SN 2012F	0.030	Ib	7.86±0.30	-1.63±0.36	7.74±0.30	-1.75±0.36	0.64±0.06
SN 2012W	0.018	II	10.05±0.03	0.30±0.07	7.70±0.03	-2.05±0.07	7.34±0.03
SN 2012al	0.040	IIn	9.77±0.17	0.01±0.26	7.62±0.17	-2.13±0.26	6.66±0.11
SN 2012bg	0.033	II P	8.29±0.16	-1.30±0.20	7.95±0.16	-1.64±0.20	0.89±0.06
SN 2012br	0.019	II P	7.40±0.34	-1.96±0.37	7.13±0.34	-2.23±0.37	0.72±0.05

Name	z	Type	Mass ($\log M_{\odot}$)	SFR (phot) ($\log M_{\odot} \text{ yr}^{-1}$)	Σ_M ($\log M_{\odot} \text{ kpc}^{-2}$)	Σ_{SFR} ($\log M_{\odot} \text{ yr}^{-1} \text{ kpc}^{-2}$)	r_{50} (kpc)
SN 2012ch	0.009	II P	8.30±0.04	-1.20±0.07	7.72±0.04	-1.78±0.07	1.52±0.02
SN 2012cr	0.010	II	9.95±0.03	0.00±0.07	8.45±0.03	-1.50±0.07	3.82±0.01
SN 2012cz	0.036	IIn	10.35±0.03	0.30±0.07	8.66±0.03	-1.39±0.07	4.85±0.02
SN 2012dp	0.036	Ib	10.59±0.04	0.82±0.12	8.00±0.04	-1.76±0.12	8.58±0.07
SN 2012ed	0.015	II	7.32±0.17	-2.01±0.42	7.32±0.17	-2.01±0.42	0.80±0.12
SN 2012ex	0.023	Ib	10.45±0.03	0.70±0.07	8.48±0.03	-1.27±0.07	4.07±0.01
SN 2012fc	0.023	II P	9.80±0.03	0.29±0.07	8.19±0.03	-1.32±0.07	3.82±0.02
SN 2012hw	0.038	II P	9.90±0.11	0.19±0.15	7.49±0.11	-2.22±0.15	6.59±0.05
SN 2012il	0.175	Ic	9.03±0.16	-0.59±0.20	8.18±0.16	-1.44±0.20	1.93±0.63
SN 2013an	0.014	II	0.32±0.25
SN 2013aw	0.027	II	9.45±0.19	-0.30±0.24	7.80±0.19	-1.95±0.24	6.63±0.06
SN 2013bn	0.054	Ic	0.78±0.13
SN 2013br	0.074	II	9.15±0.10	-0.47±0.19	8.14±0.10	-1.48±0.19	1.73±0.22
SN 2013bw	0.038	II P	10.60±0.03	1.10±0.07	8.15±0.03	-1.35±0.07	7.61±0.03
SN 2013dn	0.056	IIn	10.70±0.03	1.20±0.07	8.59±0.03	-0.91±0.07	5.50±0.06

NOTE. — Column “ z ” shows the spectroscopic redshift of the SN or LGRB, while “Type” lists the spectroscopic classification of the SN. The “Mass” and “SFR (phot)” columns are, respectively, the galaxy stellar mass and SFR we estimate by fitting broadband photometry with PEGASE2 (Fioc & Rocca-Volmerange 1999) stellar population synthesis models. Column Σ_{SFR} is the projected SFR surface density $\Sigma_{\text{SFR}} = \log_{10}(\text{SFR} / 2 / \pi AB)$ where SFR is the value estimated from photometry in the adjacent column, while A and B are the semimajor and semiminor axes (in kpc) of the isophotal ellipse that contains half of the galaxy r -band flux. The column “ r_{50} ” shows the the weighted average of the half-light radii of the de Vaucouleurs and an exponential components fit to the galaxy light distribution by the SDSS `photo` pipeline.

TABLE 3
PROPERTIES OF HOST GALAXIES WITH SDSS SPECTRA

Name	z	Type	Mass ($\log M_{\odot}$)	σ_{vel} (km s^{-1})	SFR (spec) ($\log M_{\odot} \text{ yr}^{-1}$)	Σ_{SFR} ($\log M_{\odot} \text{ yr}^{-1} \text{ kpc}^{-2}$)	Fraction deV.
PTF 09awk	0.062	Ib	9.54±0.06	63.7±0.7	-0.03±0.14	-1.00±0.14	1.0
PTF 09dra	0.077	II	10.50±0.08	77.1±2.6	0.30±0.33	-2.46±0.33	0.5
PTF 09ige	0.064	II	9.73±0.06	44.2±1.2	0.21±0.25	-1.93±0.25	0.2
PTF 09ism	0.029	II	9.12±0.21	33.2±3.1	-0.68±0.40	-2.42±0.40	0.2
PTF 09sk	0.036	Ic-BL	8.93±0.15	51.4±0.7	-0.40±0.22	-1.48±0.22	0.5
PTF 09uj	0.065	II	9.75±0.08	52.7±3.4	-0.08±0.27	-2.17±0.27	0.0
PTF 10bau	0.026	II	10.75±0.03	80.8±1.1	0.41±0.22	-1.62±0.22	0.2
PTF 10bhu	0.036	Ic	9.43±0.14	51.0±2.1	-0.27±0.29	-1.92±0.29	0.0
PTF 10con	0.033	II	9.68±0.16	68.6±2.3	-0.60±0.30	-1.96±0.30	0.1
PTF 10cxx	0.034	II	10.03±0.13	68.2±1.0	-0.07±0.18	-1.46±0.18	0.2
PTF 10s	0.051	II	9.66±0.09	38.7±1.3	-0.25±0.24	-1.90±0.24	0.0
PTF 11cgx	0.034	II	9.95±0.04	57.6±1.6	-0.00±0.26	-1.75±0.26	0.0
PTF 11cwi	0.056	II	10.58±0.09	110.9±1.2	0.70±0.13	-1.33±0.13	1.0
PTF 11dqk	0.036	II	9.81±0.04	42.5±0.8	0.35±0.23	-1.56±0.23	0.1
PTF 11dd	0.040	II	10.38±0.04	69.0±3.6	-0.39±0.78	-2.89±0.78	0.0
PTF 11ecp	0.034	II	10.15±0.12	53.9±1.3	0.25±0.30	-1.71±0.30	0.0
PTF 11gdz	0.013	II	9.89±0.29	68.0±0.5	-0.34±0.13	-1.36±0.13	0.1
PTF 11jgp	0.072	II	10.02±0.06	55.0±1.3	0.28±0.25	-1.70±0.25	0.0
PTF 11mpv	0.043	II	9.27±0.11	41.1±1.4	-0.47±0.22	-1.56±0.22	0.4
PTF 11qem	0.051	II	10.65±0.09	83.7±2.2	0.01±0.32	-2.19±0.32	0.0
PTF 11qu	0.028	II	9.35±0.19	37.6±1.3	-0.32±0.23	-2.22±0.23	0.0
PTF 11qux	0.041	II	9.58±0.11	48.0±0.7	-0.14±0.13	-1.23±0.13	0.0
PTF 12cgb	0.026	II	9.29±0.20	49.3±0.8	-0.30±0.27	-1.58±0.27	0.1
PTF 12dke	0.067	II	9.83±0.09	57.7±3.0	0.18±0.30	-2.32±0.30	0.1
PTF 12eje	0.078	II	9.86±0.09	49.8±1.5	-0.64±0.16	-2.75±0.16	0.0
PTF 12gcx	0.045	II	9.67±0.16	39.4±1.2	-0.96±0.35	-3.28±0.35	0.1
PTF 12gzk	0.014	12gzk	7.29±0.09	59.0±0.7	-2.40±0.09	-2.45±0.09	1.0
PTF 13c	0.011	II	8.68±0.30	49.4±1.4	-0.68±0.33	-1.72±0.33	0.0
PTF 13cbf	0.040	Ic	9.51±0.14	47.0±0.4	0.26±0.20	-1.44±0.20	0.2
SN 2004hy	0.058	II	9.69±0.11	46.4±4.4	-0.16±0.31	-2.54±0.31	0.2
SN 2005hl	0.023	Ib	10.43±0.18	63.8±1.1	0.16±0.22	-1.46±0.22	0.0
SN 2005kb	0.015	II	9.14±0.38	28.6±1.4	-1.00±0.30	-2.16±0.30	0.0
SN 2005ks	0.099	Ic-BL	9.89±0.07	70.4±1.4	-0.10±0.24	-1.53±0.24	0.0
SN 2005lc	0.014	II	8.50±0.34	34.8±3.1	-1.53±0.27	-2.59±0.27	0.1
SN 2005lm	0.085	II	9.33±0.08	43.7±1.1	-0.60±0.08	-1.87±0.08	0.3
SN 2005mn	0.047	Ib	9.52±0.13	44.2±2.6	-0.17±0.30	-2.27±0.30	0.2
SN 2006M	0.015	IIIn	8.86±0.29	43.9±2.1	-0.64±0.24	-1.96±0.24	0.1
SN 2006bj	0.038	II	9.40±0.14	43.9±2.9	-1.57±0.23	-3.63±0.23	0.2
SN 2006cw	0.061	II	9.87±0.08	49.7±1.6	0.13±0.27	-2.02±0.27	0.0
SN 2006db	0.023	IIIn	8.69±0.21	46.4±3.0	-0.92±0.27	-2.21±0.27	0.2
SN 2006fo	0.021	Ib	10.65±0.03	61.3±0.8	0.05±0.24	-1.67±0.24	0.1
SN 2006fq	0.068	II P	10.04±0.04	46.1±0.4	0.32±0.25	-1.48±0.25	0.1
SN 2006gd	0.155	II P	11.02±0.06	101.9±7.8	-0.33±1.00	-3.10±1.00	0.6
SN 2006iw	0.031	II	9.73±0.15	34.2±2.0	-0.52±0.36	-2.15±0.36	0.0
SN 2006ix	0.076	II	9.57±0.08	48.3±2.5	-1.01±0.15	-2.81±0.15	0.1
SN 2006kh	0.060	II	9.47±0.10	65.5±1.0	-0.70±0.10	-1.18±0.10	0.3
SN 2006kn	0.120	II	10.08±0.16	51.6±3.4	-0.30±0.39	-2.52±0.39	0.0
SN 2006ns	0.120	II	9.88±0.06	43.4±1.8	0.33±0.26	-1.71±0.26	0.2
SN 2006qk	0.058	Ic-BL	9.55±0.11	57.4±1.4	-0.60±0.13	-1.30±0.13	0.1
SN 2007I	0.022	Ic-BL	8.82±0.20	42.7±2.9	-1.07±0.29	-2.20±0.29	0.0
SN 2007bo	0.044	II	9.11±0.12	41.6±2.5	-0.44±0.35	-2.29±0.35	0.1
SN 2007bp	0.028	II	10.60±0.04	46.0±4.3	-1.61±1.11	-4.36±1.11	0.4
SN 2007dp	0.033	II	9.19±0.14	43.8±1.6	-0.62±0.27	-1.82±0.27	0.0
SN 2007fe	0.033	II	9.59±0.17	53.1±1.2	-0.33±0.23	-1.92±0.23	0.3
SN 2007fg	0.026	II	8.84±0.19	37.7±0.8	-0.60±0.21	-2.22±0.21	0.0

Name	z	Type	Mass ($\log M_{\odot}$)	σ_{vel} (km s^{-1})	SFR (spec) ($\log M_{\odot} \text{ yr}^{-1}$)	Σ_{SFR} ($\log M_{\odot} \text{ yr}^{-1} \text{ kpc}^{-2}$)	Fraction deV.
SN 2007fy	0.045	II	10.03±0.11	59.2±0.8	0.27±0.25	-1.61±0.25	0.1
SN 2007ib	0.034	II	10.00±0.14	57.1±0.9	0.12±0.25	-1.84±0.25	0.1
SN 2007jf	0.070	II P	9.56±0.10	44.6±2.2	-1.07±0.12	-2.94±0.12	0.4
SN 2007jm	0.091	II n	9.70±0.10	56.9±1.8	-0.55±0.13	-2.00±0.13	0.3
SN 2007ky	0.074	II	11.03±0.07	79.4±4.4	0.47±0.45	-2.41±0.45	0.6
SN 2007lx	0.058	II	10.72±0.10	69.2±2.7	0.79±0.33	-1.46±0.33	0.8
SN 2007nw	0.057	II P	10.26±0.10	74.9±1.8	0.09±0.33	-1.93±0.33	0.6
SN 2007qb	0.079	II	10.27±0.05	70.2±1.3	0.67±0.26	-2.06±0.26	0.6
SN 2007qw	0.151	Ic-BL	9.36±0.08	49.1±1.0	-0.09±0.08	-1.18±0.08	0.7
SN 2008bj	0.019	II	8.49±0.32	27.3±2.5	-0.80±0.23	-2.42±0.23	0.0
SN 2008fo	0.030	Ic	9.49±0.20	52.2±0.8	0.03±0.22	-1.76±0.22	0.0
SN 2008gd	0.059	II	9.89±0.09	41.3±3.4	-0.01±0.34	-2.48±0.34	0.2
SN 2009bk	0.039	II	9.80±0.15	44.8±1.4	0.16±0.31	-1.74±0.31	0.0
SN 2009bl	0.040	II	9.85±0.04	54.4±2.2	0.14±0.27	-1.58±0.27	0.0
SN 2009ct	0.057	II	10.58±0.08	97.4±3.1	0.42±0.34	-1.85±0.34	0.6
SN 2010ay	0.067	Ic-BL	8.55±0.09	61.3±0.6	-0.01±0.12	0.32±0.12	1.0
SN 2011bm	0.022	Ic	9.85±0.04	57.1±0.8	-0.04±0.23	-1.63±0.23	0.3
SN 2011cq	0.017	II pec	9.97±0.33	67.9±2.4	-0.65±0.42	-2.94±0.42	0.4
SN 2011en	0.018	II P	8.51±0.32	12.7±7.5	-1.07±0.24	-2.37±0.24	0.1
SN 2011hn	0.014	II P	9.95±0.04	12.6±2.8	-0.52±0.41	-2.35±0.41	0.2
SN 2011jm	0.003	Ic	8.82±0.06	31.9±0.3	-2.51±0.15	-3.23±0.15	0.4
SN 2012D	0.026	II P	9.65±0.03	47.4±0.5	0.14±0.21	-1.34±0.21	0.0
SN 2012al	0.038	II n	9.55±0.17	34.8±3.9	-1.49±1.01	-3.59±1.01	0.0
SN 2012dp	0.036	Ib	10.55±0.03	85.4±0.8	0.56±0.17	-2.02±0.17	0.9
SN 2012ex	0.023	Ib	8.77±0.37	21.2±0.8	-1.49±0.11	-3.58±0.11	0.3
SN 2012hw	0.038	II P	10.06±0.13	39.4±2.4	0.05±0.31	-2.36±0.31	0.0
SN 2013aw	0.027	II	9.37±0.21	40.3±1.2	-0.57±0.26	-2.21±0.26	0.1

NOTE. — Column “ z ” shows the SN spectroscopic redshift, while “Type” lists the spectroscopic classification. The “Mass” column shows the galaxy stellar mass we estimate by fitting broadband photometry with PEGASE2 (Fioc & Rocca-Volmerange 1999) stellar population synthesis models. The σ_{vel} estimate is of the gas velocity dispersion measured from the $\text{H}\alpha$ emission-line profile by the Portsmouth group (Thomas et al. 2013) using the Penalized PiXel Fitting (Cappellari & Emsellem 2004) (pPXF) and the Gas and Absorption Line Fitting (Sarzi et al. 2006) (GANDALF v1.5) codes. The column “SFR (spec)” is a hybrid SFR estimate computed by the MPA-JHU group that is the sum of the SFR inside the SDSS fiber aperture inferred from the spectrum, and the SFR outside of the aperture from modeling *ugriz* photometry. Column Σ_{SFR} is the projected SFR surface density $\Sigma_{\text{SFR}} = \log_{10}(\text{SFR} / 2 / \pi AB)$ where SFR is the hybrid value in the adjacent column, while A and B are the semimajor and semiminor axes (in kpc) of the isophotal ellipse that contains half of the galaxy r -band flux. The column “Fraction deV.” shows the fraction of the total galaxy light attributed to the de Vaucouleurs $r^{1/4}$ component from a simultaneous fit by the SDSS `photo` pipeline of a de Vaucouleurs and an exponential profile to the galaxy light distribution.